Fundamental Palladium Catalyzed Oxidative Addition Reactions

By
Bryan Phuti Moloto

Dissertation presented for the degree of Doctor of Philosophy in the Faculty of Science at Stellenbosch University

Supervisor: Prof. Catharine Esterhuysen
Supervisor: Prof. F. Matthias Bickelhaupt
Co-supervisor: Dr. Trevor A. Hamlin

December 2023

Fundamental Palladium Catalyzed Oxidative Addition Reactions

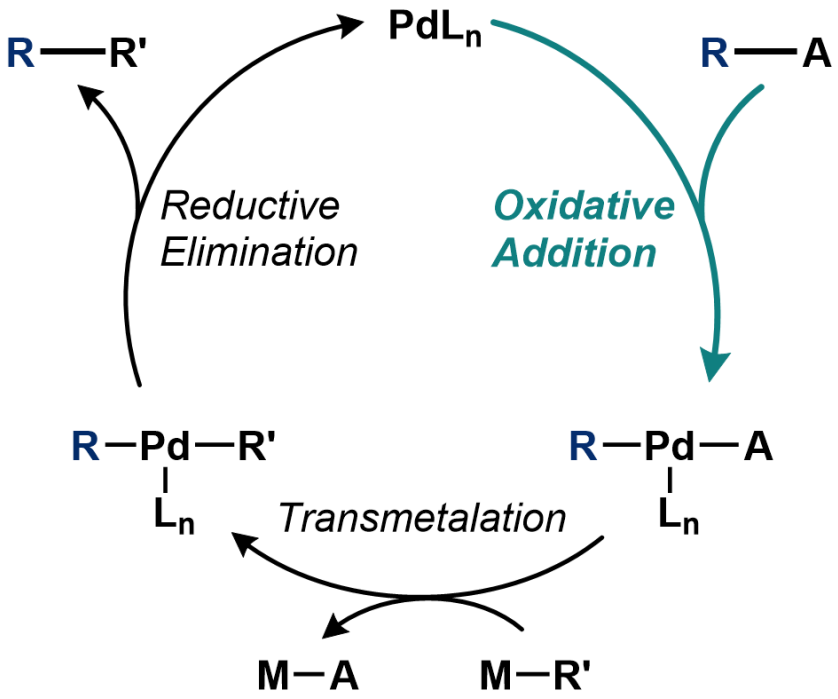

Bryan Phuti Moloto

VRIJE UNIVERSITEIT

FUNDAMENTAL PALLADIUM CATALYZED OXIDATIVE ADDITION REACTIONS

ACADEMISCH PROEFSCHRIFT

ter verkrijging van de graad Doctor of Philosophy aan
de Vrije Universiteit Amsterdam,
op gezag van de rector magnificus
prof.dr. J.J.G. Geurts,
in het openbaar te verdedigen
ten overstaan van de promotiecommissie
van de Faculteit der Bètawetenschappen
op maandag 16 oktober 2023 om 11.45 uur
in een bijeenkomst van de universiteit,
De Boelelaan 1105

door

Bryan Phuti Moloto

geboren te Polokwane, Zuid-Afrika

promotoren:	prof.dr. F.M. Bickelhaupt prof.dr. C. Esterhuysen
copromotor:	dr. T.A. Hamlin
promotiecommissie:	prof.dr. T.N. Grossmann prof.dr. J. Poater prof.dr. L. Orian prof.dr. T.C. Ramalho prof.dr. J. Dillen dr. T. Hansen

Declaration

By submitting this dissertation electronically, I declare that the entirety of the work contained therein is my own, original work, that I am the sole author thereof (save to the extent explicitly otherwise stated), that reproduction and publication thereof by Stellenbosch University will not infringe any third party rights and that I have not previously in its entirety or in part submitted it for obtaining any qualification.

December 2023

This work has been financially supported by the National Research Foundation of South Africa (NRF, UID grant no. 115979 and CPRR grant no. 141992), Nuffic's Netherlands Education Support Office (NESO), and Netherlands Organization for Scientific Research (NWO). Opinions expressed and conclusions arrived at, are those of the author and are not necessarily to be attributed to the Funders.

Fundamental Palladium Catalyzed Oxidative Addition Reactions

Bryan Phuti Moloto

2023

"All theoretical chemistry is really physics, and all theoretical chemists know it."

Richard P. Feynman

Table of Contents

Chapter 1

Introduction

1.1 Theoretical Chemistry

Theoretical chemistry is a scientific discipline centered on the development of broad theoretical generalizations. It is progressing at a wonderful rate and rising enormously due to the availability of computational resources. Historically, chemists would rely exclusively on their laboratory observations to understand the molecular world. Today, however, they have access to modern quantum chemical tools that they can utilize as a reliable alternative to support and rationalize their experimental findings. Software and models for computational chemistry enable an accurate description of a wide range of chemical systems as well as a better and more in-depth understanding of chemical phenomena based on first principles.[1] The experimental reaction conditions and other crucial laboratory parameters can be modelled. Many scientists now have more ability to comprehend chemical reactions from a theoretical perspective thanks to modern discoveries. Density Functional Theory (DFT) research has greatly contributed to our understanding of quantum chemistry.[2] Through the use of theoretical physics techniques, quantum chemistry can explain chemical phenomena.[3] In this area, the main theory used to predict the kinetic and thermodynamic features of chemical systems is quantum mechanics.[4] One can extract important information from reactions of interest such as the potential energy surfaces and how they emerge from the underlying molecular-orbital electronic structure of the reactants, using the appropriate computational tools in theoretical chemistry. Upon reading this thesis, the interested reader will, therefore, gain an understanding of chemical reactivity based on a pure theoretical footing.

In many catalytic processes, palladium is utilized as a catalyst, particularly in cross-coupling reactions. The focus of this thesis is on the broad and important topic of catalysis, in particular, the bond-activation step in homogeneous catalysis (where the reacting species are dissolved in one medium). It is frequently challenging to rationalize the reactivity of catalytic agents despite various pioneering contributions from various areas of the molecular sciences.

In particular, it is challenging to predict a proposed catalyst's activity. Therefore, most catalysts are found and developed through laborious trial-and-error approaches that consume much time and resources. It becomes even more problematic in the field of homogeneous catalysis in which the role of the ligands can become very complex and, in some cases, may even drastically change the mechanism of action of the studied models.

With the help of computational chemistry, theoreticians can gain a better insight into reaction mechanisms. By doing so, theoreticians aim to broaden and enhance the "chemical intuition" that chemists use to explain but also to predict this reactivity. One approach is to start with straightforward, archetypical model systems and then, in a stepwise fashion, introduce more complexity until the essential components of real-world catalytic systems are achieved.[5-8] In this way, the role of each component of the reaction system can be determined and understood in great detail. This is the approach of the present work.

1.2 Oxidative Addition of Palladium

Palladium (Pd) belongs to the class of precious metals (PGMs), and because of the growing demand for it in a variety of essential industrial applications, its market price is currently (as of the draft of this thesis in 2022) around $1,900 per ounce, which is slightly more expensive than gold.[9] Pd is widely employed in catalytic converters where it serves as the main element, along with smaller amounts of platinum and rhodium, for the reduction of light hydrocarbons, carbon monoxide, oxides of nitrogen, and other polluting emissions from vehicle exhausts. It has also been widely utilized in jewelry and electronics and as a component in dental alloys. In addition to these uses, Pd is a common and adaptable catalytic reagent in a wide range of chemical processes.[10] One reason why this thesis focuses on Pd is that it can serve excellently as a model system. The atomic ground state of Pd consists of a closed-shell d^{10} configuration, which facilitates comparison with larger, more realistic transition-metal complexes used in catalytic bond activation, thus making palladium oxidative addition reactions highly relevant in catalysis.

Murahashi was the first to discover the importance of Grignard reagents as nucleophiles in Pd-catalyzed cross coupling reaction.[11,12] Thereafter, Negishi showed the importance of several organometallic compounds,[13] and many began to showcase the ability of these Pd-

based compounds to participate as nucleophiles in cross-coupling processes.[14-16] Negishi nicely illustrated that iodobenzene selectively couples with different functional groups through a Pd-catalyzed addition-elimination series.[17] The Suzuki reaction is another indispensable Pd-catalyzed carbon–carbon bond-forming reaction involving the Pd-mediated coupling of organic electrophiles.[18,19] This reaction is the refinement of the well-known Heck and Negishi reactions.[13,20]

In recent years, Diefenbach *et al.* demonstrated the advantage of utilizing a stable closed-shell d^{10} ground state Pd and established that relativistic effects are important for an accurate quantum chemical description of the oxidative addition. Most importantly, the study has shown that the relativistic effects in metal-catalyzed bond activations substantially stabilize the stationary points along the potential energy surface (PES) and that both the barrier heights and reaction energies become more negative.[21,22,27,28] In their earlier investigations of oxidative insertion processes, de Jong *et al.* conducted a thorough theoretical investigation of the Pd-induced activation of carbon–element bonds with more focus on comprehending the mechanism and the trends in reactivity of the oxidative addition reactions.[23–28] This work showed that ZORA-BLYP/TZ2P was a suitable computational method for the study of these reactions. Demonstrating and showcasing the theoretical model of Pd's activation of carbon–element bonds by unravelling the effects of hybridization (mainly by variating the hybridization and not by variating the substituent X in C(sp^n)–X (n = 1–3)), and the trends therein, Hansen *et al.* recently built a strong theoretical framework for understanding the C(sp^n)–X (n = 1–3) activation by Pd and have found that the higher reactivity in their reaction models is not controlled by the bond strength, but by the relief in the steric (Pauli) repulsion found between the catalyst and the substrate (selected reaction models).[29,30(a)] The main motivation for this thesis focuses on palladium because it can serve excellently as a desired model system. Palladium is widely used in catalytic processes.[30(b–d] Crucial examples are the oxidation of alkenes by the $PdCl_2/CuCl_2$ system (Wacker process) or the activation by palladium complexes of aryl-halogen bonds for C–C coupling reactions (Heck reaction).[30(e,f)] The atomic ground state of Pd consists of a closed-shell d^{10} configuration, which facilitates comparison with more realistic transition metal complexes used in catalytic bond activation as these are in general (although not always) closed-shell species.[30(g–i)]

We have chosen relatively simple model systems in order to focus on the development of computational approaches and of analytical models to rationalize the reactivity. This is of interest also for industrial chemistry because it enables a more rational design of catalytically active species. One example is the activation and subsequent functionalization of the rather

inert alkanes (e.g. CH_4).[30b] Whereas the long-term purpose of our efforts is understanding and directing, in a rational manner, the factors that determine the catalytic activity and selectivity of transition metal *complexes*, the starting point is the investigation of the *intrinsic* reactivity of the transition metal *atom*. Thus, by introducing ligands in a second stage, it can be precisely assessed how they interfere with the metal electronic structure and how they exactly affect the activity and selectivity of the resulting homogeneous catalyst. The studies motivated our research goals in achieving the aim of this research project – that is, to study the mechanisms of action of Pd-based catalysts in a series of bond-activation processes. Our findings can be dissected in more detail in chapters three (3) and four (4) of this thesis.

The abundant study of theoretical oxidative insertion reactions by Pd has indeed been proven to be useful in understanding the mechanism behind it, and has been mimicked by Sun *et al*. through their intensive theoretical rational design techniques utilising iron-based catalysts to investigate the capabilities in C–X bond activation and interestingly similar mechanisms and trends in reactivity in iron based models were observed.[31,32]

In addition to the aforementioned significant "track record of studies" of the C–X bond activation by Pd, all the systems chosen in this thesis were chosen to address the concept of an oxidative addition reaction in which a reactant (substrate) adds to a metal complex from the separate reactants (R) through a reactant complex (RC) and a transition state (TS) to obtain the product complex (PC).[33–36] Oxidative addition embraces a ubiquitous class of reactions in which a reactant adding to a metal complex oxidizes it. For example, oxidative addition of a molecule R–A to Pd(0) leads to the cleavage of the covalent bond between R and A and the formation of two new bonds: R–Pd–A (see Scheme 1.1). Two previously nonbonding electrons of Pd are involved, yielding an increase in the formal oxidation state by two: Pd(0) is oxidized to Pd(II).

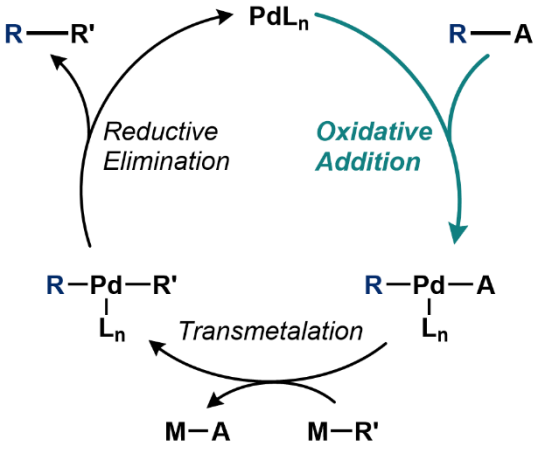

Scheme 1.1. Schematic catalytic cycle of a palladium-catalyzed cross-coupling reaction.

This thesis aims to study, investigate, and understand the mechanism of the oxidative addition step involving Pd with several archetypal organic substrates. This concerted mechanism, is fundamental for understanding carbon–element bond activations by Pd.[21,30(a),31,32]

Since ligands have the potential to change how the metal center acts, it is imperative to look at their effects. The concept of ligands will be fully addressed in Chapter 4 of this thesis. Mono- and bi-coordinated phosphine ligands have proven to raise the potential energy surface, while the anion-assisted ligands tend to improve or stabilize it[37] thus improving the catalytic activity. van Zeist *et al.* conducted a thorough quantum chemical analysis paying particular attention to "bite angles", that is, the ligand-metal-ligand angle (LML) of various chelate ligands.[37,38] It has been demonstrated that the LML angle has a considerable impact on the catalyst's activity, either decreasing or enhancing it.

1.3 This Thesis

The overarching aim of this research is to study the mechanisms of action of Pd-based catalysts in a series of bond-activation processes. In particular, the aim is to investigate the nature of the oxidative addition reaction, a key step, often rate-determining in many catalytic cycles, in which a reactant (substrate) adds to a metal complex, forming the reactant complex that then continues to a transition state that connects both the reactant complex and the product complex.

The research objectives are to:

(a) Investigate the oxidative addition of archetypical carbon–halogen bonds to palladium and determine how these reactions depend on the s–p hybridization of the pertinent carbon atom.

(b) Investigate the oxidative addition of archetypical second-period element–element bonds to palladium and, proceeding from there, uncover the effect of introducing ligands.

(c) Analyze the potential minimum energy pathways of all model reactions using the activation strain model in combination with quantitative Kohn–Sham Molecular Orbital (KS-MO) Theory and energy decomposition analysis (EDA) to unveil their nature and to understand how the underlying physical factors determine the overall trends.

(d) Disseminate the resulting information and insights to help experimentalists develop better catalytic processes.

The first chapter of the current manuscript serves as an introduction to shed light on a broader concept of Theoretical Chemistry, Pd as a metal, and the oxidative addition reaction step in cross-coupling processes. Chapter 2 provides a brief overview of the key theoretical methods and models used; it is divided into three sections (see Sections 2.1, 2.2, and 2.3, wherein we describe the concept of quantum chemistry based on the Schrödinger's equation, followed by a description of density functional theory, and explaining the activation strain model of chemical reactivity, respectively).

Chapter 3 describes the quantum chemical studies of the Pd-mediated activation of C(sp^n)–X bonds (n = 1–3; X = F, Cl, Br, I) in the archetypal model substrates $H_3C–CH_2–X$, $H_2C=CH–X$, and $HC\equiv C–X$ by a model bare palladium catalyst using relativistic Density Functional Theory at ZORA-BLYP/TZ2P.

Turning to Chapter 4, we have, through quantum chemical analyses, investigated the Pd-mediated activation of $H_nA–AH_n$ bonds (AH_n = CH_3, NH_2, OH, F) by catalysts PdL_n with L_n = no ligand, PH_3, $(PH_3)_2$, using relativistic Density Functional Theory at ZORA-BLYP/TZ2P.

To conclude, the summary of the thesis is provided in English, Dutch (samenvatting), and Afrikaans (opsomming). After this, come the acknowledgements and a list of publications.

1.4 References

[1] C.J. Cramer, *Essentials of Computational Chemistry: Theories and Models,* New York, Wiley, **2002**.

[2] R.G. Parr, W. Yang, *Density-Functional Theory of Atoms and Molecules*, Oxford Science Publications, **1989**.

[3] J. Simons, J. Nichols, *Quantum Mechanics in Chemistry,* New York, Oxford University Press, **1997**.

[4] P.W. Atkins, R.S. Friedman, *Molecular Quantum Mechanics*, 3rd edition, New York, Oxford University Press, **1996**.

[5] A. Diefenbach, *Fragment-orientated Design of Catalysts. A theoretical study on bond activation*, Doctoral Dissertation, Philipps-Universität, Marburg, **2000**.

[6] G.T. de Jong, *Theoretical Studies on Catalytic Bond Activation*, Doctoral Dissertation, Vrije Universiteit, Amsterdam, **2007**.

[7] W.-J. van Zeist, *Activating Bonds: The Theoretical Studies of Chemical Bonds and their Catalytic Activations by Palladium*, Doctoral Dissertation, Vrije Universiteit, Amsterdam, **2011**.

[8] X. Sun, *Activating Bonds: Rational Design of Iron-Based Catalysts for Cross-Coupling*, Doctoral Dissertation, Vrije Universiteit, Amsterdam, **2019**.

[9] *"Live Palladium Spot Prices",*

https://www.monex.com/palladium-prices/

[10] J.C. Fiaud, J.L. Malleron, J.Y. Legros, *Handbook of Palladium Catalyzed Organic Reactions*, London, Academic Press, **1997**.

[11] N. Miyaura, A. Suzuki, *Chem. Rev*. **1995**, *95*, 2457.

[12] M. Yamamura, I. Moritani, S.J. Murahashi, *J. Organomet. Chem.* **1975**, *91*, C39.

[13] E. Negishi, *Aspects of Mechanism and Organometallic Chemistry*, Brewster, J. H. Ed., New York, Plenum Press, **1978**.

[14] S. Murahashi, M. Yamamura, K. Yanagizawa, N. Mita, K. Kondo, *J. Org. Chem*. **1979**, *44*, 2408.

[15] M. Kosugi, Y. Simizu, T. Migita, *Chem. Lett*. **1977**, 1423.

[16] D. Milstein, J.K. Stille, *J. Am. Chem. Soc*. **1979**, *101*, 4992.

[17] A.O. Aliprantis, J.W. Canary, *J. Am. Chem. Soc*. **1994**, *116*, 6985

[18] K.C. Nicoolaou, P.G. Bulger, D. Sarlah, *Angew. Chem. Int. Ed*. **2005**, *44*, 4442.

[19] A. Suzuki, *Acc. Chem. Res*. **1982**, *15*, 178.

[20] H.A. Dieck, R. F. Heck, *J. Org. Chem*. **1975**, *40*, 1083.

[21] A. Diefenbach, F.M. Bickelhaupt, *J. Chem. Phys*. **2001**, *115*, 4030.

[22] A. Diefenbach, F.M. Bickelhaupt, *J. Organomet. Chem.* **2005**, *690*, 2191.

[23] G.T. de Jong, M. Solà, L. Visscher, F.M. Bickelhaupt, *J. Chem. Phys.* **2004**, *121*, 9982.

[24] G.T. de Jong, D. P. Geerke, A. Diefenbach, F.M. Bickelhaupt, *J. Chem. Phys.* **2005**, *313*, 261.

[25] G.T. de Jong, D.P. Geerke, A. Diefenbach, M. Solà, F.M. Bickelhaupt, *J. Comput. Chem.* **2005**, *26*, 1006.

[26] G.T. de Jong, F.M. Bickelhaupt, *J. Phys. Chem. A.* **2005**, *109*, 9685.

[27] G.T. de Jong, Attila Kova´cs, F.M. Bickelhaupt, *J. Phys. Chem. A.* **2006**, *110*, 7943.

[28] G.T. de Jong, F.M. Bickelhaupt, *J. Chem. Theory Comput*. **2007**, *3*, 514.

[29] T. Hansen, X. Sun, M. Dalla Tiezza, W. -J. van Zeist, J. N. P. van Stralen, D. P. Geerke, L. P. Wolters, J. Poater, T. A. Hamlin, F.M. Bickelhaupt, *Chem. Eur. J.* **2022**, *28*, e202201093.

[30] a) T. Hansen, X. Sun, M. Dalla Tiezza, W.-J. van Zeist, J. Poater, T.A. Hamlin, F.M. Bickelhaupt, *Chem. Eur. J.* **2022**, *28*, e202103953. b) A. Basile, S. Fasson, G. Vitulli, E. Drioli, *Stud. Surf. Sci. Catal*. **1998**, *119*, 453. c) J.L. Malleron, J.C. Fiaud, J.Y Legros, Handbook of Palladium Catalyzed Organic Reactions; Academic Press, **1997**. d) R. Cornils, W.A. Herrmann, Applied Homogenous Catalysis with Organometallic Compounds. Vol. 1; VCH: Weinheim, **1996**, p. 394. e) J. Tsuji, Palladium reagents and catalysts, Wiley, Chichester, **1995**. f) L. S., Hegedus Transition Metals in the Synthesis of Complex Organic Molecules. Second Edition, University Science Books, Sausalito, California, **1999**. g) A. Dedieu, *Chem. Rev.* **2000**, *100*, 543. h) O.V. Gritsenko, A.A. Bagatur' yants, I.I. Moiseev, V.B. Kazanskii, *Russ. Chem. Rev*. **1985**, *54*, 1151. i) P. Pyykkö, *Chem. Rev.* **1988**, *88*, 563.

[31] X. Sun, M.V.J. Rocha, T.A. Hamlin, J. Poater, F.M. Bickelhaupt, *Phys. Chem. Chem. Phys*. **2019**, *21*, 9651.

[32] X. Sun, T. Hansen, J. Poater, T.A. Hamlin, F.M. Bickelhaupt, *J. Comput. Chem*. **2022**, *44*, 495.

[33] J.P. Collman, L.S. Hegedus, J.R. Norton, R.G. Finke, *Principles and Applications of Organotransition Metal Chemistry*, Mill Valley, CA, University Science Books, **1987**.

[34] C. Elschenbroich, *Organometallics*. 3rd ed., Weinheim, Wiley-VCH, **2006**.

[35] M.B. Smith, *March's advanced organic chemistry: reactions, mechanisms, and structure*. 5th ed., New York, Wiley, **2001**.

[36] J.F. Hartwig, *Organotransition Metal Chemistry: From Bonding to Catalysis*, University Science Books, Sausalito, **2010**

[37] W.-J. van Zeist, R. Visser, F.M. Bickelhaupt, *Chem. Eur. J.* **2009**, *15*, 6112.

[38] W.-J. van Zeist, F.M. Bickelhaupt, *Dalton Trans*. **2011**, *40*, 3028.

Chapter 2

Theories, Methods, and Models

2.1 Quantum Chemistry

The Schrödinger equation [Eq. (2.1)] was one of the key discoveries that allowed researchers to access the "world" of quantum chemistry, which had previously been difficult to tap into.[1]

$$H\Psi = i\hbar\partial\Psi/\partial t \tag{2.1}$$

Ψ is the wave function and H is the Hamiltonian operator, which symbolizes and explains the wave function's dependence on total energy E. If the Hamiltonian operator remains invariant, it is possible to simplify the Schrödinger equation by splitting it into time-dependent and time-independent components, where [Eq. (2.2)] provides the time-independent Schrödinger equation.

$$H\Psi = E\Psi \tag{2.2}$$

Given a chemical system, the Hamiltonian operator describes the kinetic energy of all nuclei (T_N) and electrons (T_e), along with a potential energy term, which encompasses both the attractive interactions between the nuclei and electrons (V_{Ne}), and the repulsive nucleus-nucleus (V_{NN}) and electron-electron (V_{ee}) interactions. [Eq. (2.3)]:

$$H = T_N + T_e + V_{Ne} + V_{NN} + V_{ee} \tag{2.3}$$

The information about the state of the system depicted is included in the wave function Ψ. Unfortunately, the Schrödinger equation can only be solved exactly for one-electron systems. To find answers to relevant chemical problems, approximations are thus necessary. Due to the substantial mass difference between atomic nuclei and electrons (the mass of a proton is roughly 1800 times that of an electron), the Born-Oppenheimer[2] approximation is used. Since electrons travel considerably more quickly than nuclei, it is presumed that electrons move around fixed nuclei. Consequently, the total wave function can be separated into an

electronic and a nuclear wave function: $\Psi = \Psi_e \Psi_N$. In the electronic Hamiltonian H_e, the nucleus-nucleus repulsion has become a constant [not shown in Eq. (2.4)], and the electrons experience a fixed potential from the positively charged nuclei. On the basis of the electronic wave function (Ψ_e) [Eq. (2.4)], the Hamiltonian [Eq. (2.3)] is then simplified to the electronic Hamiltonian (H_e):

$$H_e\Psi_e = (T_e + V_{Ne} + V_{ee})\Psi_e \qquad (2.4)$$

The Hartree-Fock scheme, as a further simplification used to solve the Schrödinger equation, approximates the electronic wavefunction Ψ_e as an antisymmetric product of one-electron wave functions.[3] This scheme allows for the recovery of about 99% of the molecular system's entire energy. A source of inaccuracy in the Hartree-Fock (HF) Theory stems from the incomplete accounting of the correlation of the electrons' movement (the so-called Coulomb correlation is not considered). Unfortunately, total energies are huge quantities, and chemists are usually only interested in energy changes that are 1% or even smaller in magnitude. Hartree-Fock Theory is improved upon by additional techniques, such as the configuration interaction (CI)[4] post-HF methods and the coupled cluster (CC)[5] post-HF methods, albeit at a significantly higher computational cost. In this work to ensure accuracy, Density Functional Theory (DFT) (outlined in the next section) calculations were used, while relativistic effects were accounted for using the zeroth-order regular approximation (ZORA).[6]

2.2 Density Functional Theory

As an alternative to Wave Function Theory, a different approach has led to the development of DFT.[7,8] The work presented in this thesis is based on DFT calculations, all of which have been carried out with the Amsterdam Density Functional (ADF) program.[9] The history of DFT dates back to the 1920s with the notion based on the Thomas-Fermi[10(a,b)] model that the ground state energy of an atom may be expressed directly and alone in terms of the electron density. Hohenberg and Kohn[11] have proven that the electron density ρ uniquely determines all properties of the molecular system, including the electronic energy [Eq. (2.5)]:

$$E = E[\rho] \qquad (2.5)$$

The benefit of DFT compared with wave function methods is that the electronic energy has a functional dependence on the electron density, which is a function of only three spatial variables, while wave function methods have a functional dependence on $3n$ (n = number of electrons) spatial variables (each electron contains three spatial variables), which translates into a considerable reduction in computational cost. Kohn and Sham's DFT[12a] introduced the concept of a reference system of non-interacting electrons moving in an effective potential V_S. The Kohn-Sham potential was constructed such that the density of the reference system equals the density of the real, interacting system. Consequently, in Kohn-Sham DFT, the electronic wave function of the reference system is expressed by a single Slater determinant, consisting of one-electron wave functions. These wave functions are the Kohn-Sham (KS) orbitals φ, from which the electron density can be constructed by taking a linear combination of their densities [Eq. (2.6)], *i.e.*:

$$\rho(\mathbf{r}) = \sum_i |\varphi_i|^2 \qquad (2.6)$$

The electronic energy is then determined from the density functional [Eq. (2.7)]:

$$E[\rho(\mathbf{r})] = T_s[\rho(\mathbf{r})] + E_{Ne}[\rho(\mathbf{r})] + E_C[\rho(\mathbf{r})] + E_{XC}[\rho(\mathbf{r})] \qquad (2.7)$$

In the expression above, $T_s[\rho(\mathbf{r})]$ is the description of the kinetic energy of the electrons in the non-interacting reference system, whereas $E_{Ne}[\rho(\mathbf{r})]$ denotes the electrostatic attraction between the electron density and the nuclei. The classical Coulomb repulsion between electrons, or $E_C[\rho(\mathbf{r})]$, is the third term — it is the repulsion that each electron feels from the average field caused by all electrons, including itself. The exchange-correlation energy, or $E_{XC}[\rho(\mathbf{r})]$, is the last term and makes up for the deficiencies of $T_s[\rho(\mathbf{r})]$ and $E_C[\rho(\mathbf{r})]$.

The kinetic energy of the electrons in the Kohn-Sham reference system, $T_s[\rho(\mathbf{r})]$ is different from the kinetic energy of the real system, $T[\rho(r)]$. For the fourth term in Eq. 2.7, $E_{XC}[\rho(\mathbf{r})]$, there is no analytical expression. Thus, approximations to $E_{XC}[\rho(\mathbf{r})]$ have been developed, from the local density approximation (LDA) to the generalized gradient approximation (GGA). Nowadays, one can choose from a large variety of functionals, the quality of which determines the level of DFT applied.

The one-electron Kohn-Sham orbitals are determined by [Eq. (2.8)]:

$$h^{KS}\varphi_i = (-1/2\,\nabla^2 + V_s)\,\varphi_i = \varepsilon_i\varphi_i \qquad (2.8)$$

where the one-electron Kohn-Sham Hamiltonian operator, abbreviated h^{ks}, is made up of a kinetic energy operator and the Kohn-Sham potential V_S. This potential is made up of the potential due to the charged nuclei, the Coulomb potential (V_C) due to the charge density, and the exchange-correlation potential (V_{XC}). The orbital energies, ε_i, and the one-electron Kohn-Sham orbitals φ_i are the Kohn-Sham operator's eigenvalues and eigenfunctions. The eigenvalue problem cannot be solved exactly and as such an iterative self-consistent field (SCF) procedure is utilized. This is done using the so-called self-consistent field (SCF) procedure,[12b] wherein one starts with an initial guess of the density, from which the potentials are calculated and the KS equations are solved, yielding a set of KS orbitals from which a presumably improved density is constructed. This procedure will repeatedly be employed until the difference between the input density and output density drops below a set threshold, resulting in a converged computation within the predetermined criteria.

2.3. Activation Strain Model of Chemical Reactivity

When designing new catalysts, chemists are particularly interested in how to selectively lower the activation barrier for any reaction of interest by either enhancing the catalyst-substrate interaction or reducing the destabilizing strain experienced by the catalyst. The activation barrier for the intended reaction is the energy of the transition state (TS) relative to the reactants.

To gain broader insight, reactions can be examined using the Activation Strain model of chemical reactivity,[13] also known as the distortion/interaction model,[14-16] to acquire a comprehensive understanding of how the usage of various metals and substrates affect the activation barrier. All of the research contained in this thesis has used this model of chemical reactivity because it may be used to shed light on the characteristics of an energy profile. The Activation Strain model is a fragment-based approach for describing and comprehending the potential energy surface with regard to the reactants. It takes into account the reactants' degree of stiffness, the degree of deformation that takes place throughout the reaction, as well as their propensity to interact with one another during the oxidative addition reactions (the specific

focus of this thesis). Through this model, the total energy, $\Delta E(\zeta)$, is decomposed into the strain and interaction energies, $\Delta E_{strain}(\zeta)$ and $\Delta E_{int}(\zeta)$, respectively, along the Intrinsic Reaction Coordinate (IRC)[17] which is projected onto a reaction coordinate ζ that is critically involved in the reaction [Eq. (2.9)].

$$\Delta E(\zeta) = \Delta E_{strain}(\zeta) + \Delta E_{int}(\zeta) \quad (2.9)$$

The strain energy, $\Delta E_{strain}(\zeta)$, in this equation is used to describe the energy needed to deform the reactants from their equilibrium structure to the geometry they adopt during the reaction at any given position in the reaction coordinate. Thus, there is a high correlation between strain energy and the fragments' structural stiffness. Since the reference geometries are usually not distorted, $\Delta E_{strain}(\zeta)$ is typically destabilising. When there are significant deformations, like when the substrate experiences bond cleavage during oxidative addition, $\Delta E_{strain}(\zeta)$ might increase significantly in value. The total strain $\Delta E_{strain}(\zeta)$ can be further divided into the strain energy associated with deforming each respective reactant [Eq. (2.10)].

$$\Delta E_{strain}(\zeta) = \Delta E_{strain,\ reactant\ A}(\zeta) + \Delta E_{strain,\ reactant\ B}(\zeta) \quad (2.10)$$

With reference to [Eq. (2.9)] above, the deformed reactants interact along the reaction coordinate and this contribution is entirely accounted for by the interaction energy, $\Delta E_{int}(\zeta)$. It accounts for all chemical interactions as they arise when the deformed reactants are brought from infinitely far apart to their positions in the transition state geometry. The $\Delta E_{int}(\zeta)$ term can further be dismantled utilising a canoncial energy decomposition analysis (EDA) based on the framework of Kohn-Sham Molecular Orbital (MO) Theory,[18] into three physically meaningful terms: namely, $\Delta V_{elstat}(\zeta) + \Delta E_{Pauli}(\zeta) + \Delta E_{oi}(\zeta)$ (*vide infra*).

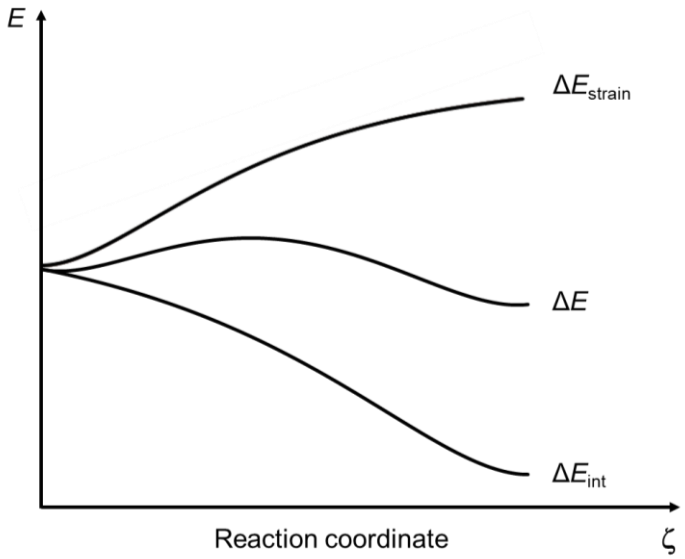

Figure 2.1. A generic representation of the activation strain model.

The Activation Strain model gives great insight into relative energies and even entire reaction energy profiles because it answers the questions of why and when a reaction barrier occurs. For instance, where the destabilization from the strain term increases at the same rate as the stabilization from the interaction energy term strengthens, namely, $d\Delta E_{\text{strain}}/d\zeta = -d\Delta E_{\text{int}}/d\zeta$the derivative of the total energy profile with respect to the reaction coordinate is zero ($d\Delta E/d\zeta = 0$). At this point, the energy profile achieves either a maximum (the reaction barrier) where the transition state occurs, or a stable minimum. The Activation Strain Model analysis can be performed to further understand the rationale behind the changes in strain and interaction energy. As mentioned already above, the ΔE_{int} can be further decomposed into three physically meaningful terms in the framework of Kohn-Sham MO theory [Eq. (2.11)]:

$$\Delta E_{\text{int}}(\zeta) = \Delta V_{\text{elstat}}(\zeta) + \Delta E_{\text{Pauli}}(\zeta) + \Delta E_{\text{oi}}(\zeta) \qquad (2.11)$$

Consider a complex AB that consists of the two fragments A and B that have electronic densities ρ_A and ρ_B, with corresponding wave functions ψ_A and ψ_B, and energies E_A and E_B, respectively. The first term in Eq. 2.11, ΔV_{elstat}, is the classical electrostatic interaction between the fragments as they are brought from infinity to their positions in the complex AB, giving rise to the density sum $\rho_{A+B} = \rho_A + \rho_B$, and corresponding Hartree product wave function $\psi_A\psi_B$. ΔV_{elstat} consists of the Coulombic repulsion between the nuclei α and β (at positions R, with

charges Z) of the fragments A and B, respectively, as well as the repulsion between their unperturbed electron densities ρ_A and ρ_B, and the attractive interactions between the nuclei of one fragment with the electron density of the other fragment [Eq. (2.12)]:

$$\Delta V_{\text{elstat}} = \sum_{\substack{\alpha\epsilon A \\ \beta\epsilon B}} \frac{Z_\alpha Z_\beta}{R_{\alpha\beta}} - \int \sum_{\alpha\epsilon A} \frac{Z_\alpha \rho^{B}(r)}{|R_\alpha - r|} \mathrm{d}r - \int \sum_{\beta\epsilon B} \frac{Z_\beta \rho^{A}(r)}{|R_\beta - r|} \mathrm{d}r + \int\int \frac{\rho^{A}(r_1)\rho^{B}(r_2)}{r_{12}} \mathrm{d}r_1 \mathrm{d}r_2 \qquad (2.12)$$

It can be established from elementary electrostatics that two interpenetrating charge clouds have a repulsion that is smaller than the one between point charges at centres, which means that fragments consisting of electronic densities around positive nuclei will typically experience a net attraction as the densities begin to overlap. Thus, ΔV_{elstat} is usually attractive (see Scheme 2.1) for molecular fragments at chemically relevant distances. The Pauli repulsion, ΔE_{Pauli}, is the energy change that occurs upon going from the product wave function $\psi_A\psi_B$ to an intermediate wave function ψ^0 that, after antisymmetrization by an operator A and renormalization by a constant N, properly obeys the Pauli principle: $\psi^0 = NA\psi_A\psi_B$. This intermediate state, with density ρ_0, has energy E^0, such that $\Delta E^0 = E^0 - E_A - E_B = \Delta V_{\text{elstat}} + \Delta E_{\text{Pauli}}$ and $\Delta E_{\text{Pauli}} = \Delta E^0 - \Delta V_{\text{elstat}}$. The Pauli repulsion accounts for the repulsive interaction between electrons having the same spin and is the origin of steric repulsion. The Pauli repulsion is responsible for, for example, the 4-electron destabilising interactions between doubly-occupied orbitals from the different fragments, as shown in Scheme 2. The requirement of antisymmetrization leads to a nodal plane in one of the two orbitals that are formed by two occupied valence orbitals from different fragments. The large gradients in a nodal plane result in a significant increase in the kinetic energy.

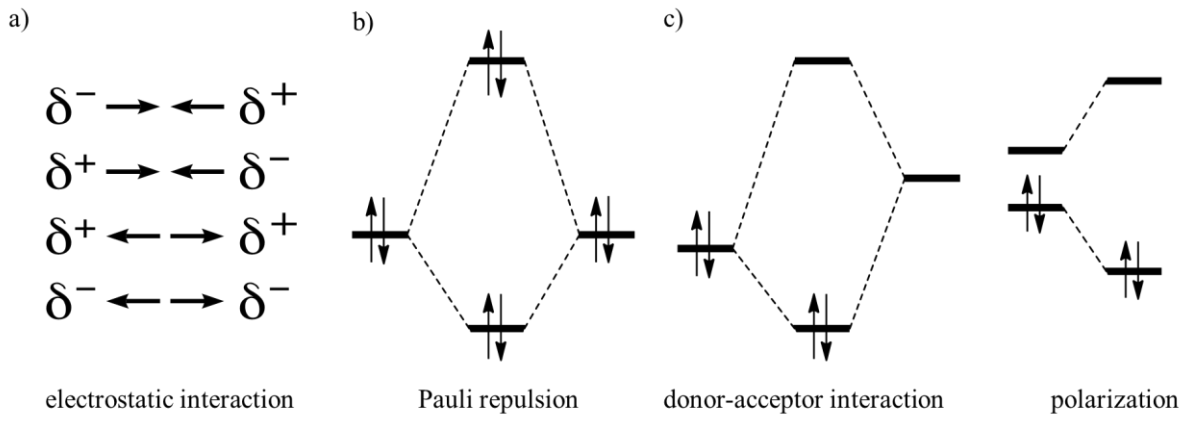

Scheme 2.1. Schematic representation of energy decomposition analysis (EDA) terms in a molecular orbital model: a) electrostatic interaction, b) Pauli repulsion, and c) orbital interactions consisting of donor-acceptor interactions and/or polarization.

In the final step, the system is allowed to relax from ψ_0, and corresponding ρ_0, to the final ψ^{AB} and optimized density ρ of the molecular complex AB. The accompanying energy change is the orbital interaction term: $\Delta E_{oi} = E^{AB} - E^0$. As a result of enabling the mixing of the fragments' virtual orbitals, this term is by definition stabilising. Due to this mixing, the orbital interaction component includes stabilising contributions from the polarization of fragments A and B as well as charge transfer between the fragments via donor–acceptor interactions. In addition, the total orbital interaction energy ΔE_{oi} can be further decomposed into contributions from each irreducible representation (irrep) Γ of the point group of the molecular system because, according to group theory, only orbitals of the same symmetry, that is, having the same character under the available symmetry operations, can interact and mix [Eq. (2.13)].

$$\Delta E_{oi} = \sum_{\Gamma} \Delta E^{\Gamma}_{oi} \qquad (2.13)$$

The Activation Strain model is performed using the PyFrag program,[19] which is a 'binder' for the Amsterdam Density Functional (ADF)[20] and allows for energy decomposition analysis (EDA) implemented in the ADF to be determined along the entire potential energy surface. The cutting-edge version of the program, PyFrag 2019,[19(a)] is also able to import the coordinates of the reaction path and directly proceed with the ADF analysis workflow using either ADF, Gaussian, ORCA, or Turbomole.

2.4 References

[1] a) F. Jensen, *Introduction to Computational Chemistry*, John Wiley & Sons, Chichester, 1999. b) C.J. Cramer, *Essentials of Computational Chemistry: Theories and Models*, John Wiley & Sons, Chichester, 2002. c) E. Schrödinger, *Ann. Phys.* **1926**, *384*, 361. d) E. Schrödinger, *Phys. Rev.* **1926**, *28*, 1049–1052. e) P.A.M. Dirac, *Proc. R. Soc. Lond. A.* **1928**, *117*, 610.

[2] M. Born, R. Oppenheimer, *Annalen der Physik.* **1927**, *389*, 457.

[3] D.R. Hartree, *Math. Proc. Camb. Philos. Soc.* **1928**, *24*, 89.

[4] U. Fano, *Phys. Rev.* **1961**, *124*, 1866.

[5] a) G.D. Purvis III, R.J. Bartlett, *J. Chem. Phys.* **1982**, *76*, 1910. b) K. Raghavachari, G.W. Trucks, J.A. Pople, M. Head-Gordon, *Chem. Phys. Lett.* **1989**, *157*, 479.

[6] a) E. van Lenthe, E.J. Baerends, J.G. Snijders, *J. Chem. Phys.* **1993**, *99*, 4597. b) E. van Lenthe, E.J. Baerends, J.G. Snijders, *J. Chem. Phys.* **1994**, *101*, 9783. c) E. van Lenthe, A. Ehlers, E.J. Baerends, *J. Chem. Phys.* **1999**, *110*, 8943.

[7] R. G. Parr, W. T. Yang, Oxford University Press, New York, 1989.

[8] W. Koch, M.C. Holthausen, *A Chemist's Guide to Density Functional Theory*, Wiley-VCH, Weinheim, 2002.

[9] a) G. te Velde, F.M. Bickelhaupt, E.J. Baerends, C. Fonseca Guerra, S.J.A. van Gisbergen, J.G. Snijders, T. Ziegler, *J. Comput. Chem.* **2001**, *22*, 931. b) C. Fonseca Guerra, J.G. Snijders, G. te Velde, E.J. Baerends, *Theor. Chem. Acc.* **1998**, *99*, 391. ADF2019.301 and ADF2019.405, SCM, *Theoretical Chemistry*, Vrije Universiteit: Amsterdam (Netherlands). http://www.scm.com.

[10] a) L.H. Thomas, *Math. Proc. Camb. Philos. Soc.* **1927**, *23*, 542. b) E. Fermi, *Z. Physik.* **1928**, *48*, 73.

[11] P. Hohenberg, W. Kohn, *Phys. Rev. B.* **1964**, *136*, B864.

[12] a) W. Kohn, L.J. Sham, *Phys. Rev.* **1965**, *140*, 1133. b) C. C. J. Roothaan, *Rev. Mod. Phys.* **1960**, *32*, 179.

[13] a) F.M. Bickelhaupt, *J. Comp. Chem.* **1999**, *20*, 114. b) W.-J. van Zeist, F.M. Bickelhaupt, *Org. Biomol. Chem.* **2010**, *8*, 3118. c) I. Fernández, F.M. Bickelhaupt, *Chem. Soc. Rev.* **2014**, *43*, 4953. d) L.P. Wolters, F.M. Bickelhaupt, *WIRES Comput. Mol. Sci.* **2015**, *5*, 324. e) F.M. Bickelhaupt, K.N. Houk, *Angew. Chem. Int. Ed.* **2017**, *56*, 10070; *Angew. Chem.* **2017**, *129*, 10204. f) P. Vermeeren, S.C.C. van der Lubbe, C. Fonseca Guerra, F.M. Bickelhaupt, T.A. Hamlin, *Nat. Protoc.* **2020**, *15*, 649.

[14] F. M. Bickelhaupt, K. N. Houk, *Angew. Chem. Int. Ed.* **2017**, *56*, 10070; *Angew. Chem.* **2017**, *129*, 10204.

[15] D.H. Ess, K.N. Houk, *J. Am. Chem. Soc.* **2007**, *129*, 10646.

[16] D.H. Ess, K.N. Houk, *J. Am. Chem. Soc.* **2008**, *130*, 10187.

[17] a) K. Fukui, *Acc. Chem. Res.* **1981**, *14*, 363. b) L. Deng, T. Ziegler, L.A. Fan, *J. Chem. Phys.* **1993**, *99*, 3823. c) L. Deng, T. Ziegler, *Int. J. Quantum Chem.* **1994**, *52*, 731.

[18] a) F.M. Bickelhaupt, E.J. Baerends, *Kohn-Sham Density Functional Theory: Predicting and Understanding Chemistry*, *In Reviews in Computational Chemistry*; K.B. Lipkowitz, D.B. Boyd, Eds., Wiley-VCH, New York, 2000, Vol. 15, pp 1. b) R. van Meer, O.V. Gritsenko, E.J. Baerends, *J. Chem. Theory Comput.* **2014**, *10*, 4432.

[19] a) X. Sun, T.M. Soini, J. Poater, T.A. Hamlin, F.M. Bickelhaupt, *J. Comput. Chem.* **2019**, *40*, 2227. b) W.-J. van Zeist, C. Fonseca Guerra, F.M. Bickelhaupt, *J. Comp. Chem.* **2008**, *29*, 312.

[20] a) G. te Velde, F.M. Bickelhaupt, E.J. Baerends, C. Fonseca Guerra, S.J.A. van Gisbergen, J.G. Snijders, T. Ziegler, *J. Comput. Chem.* **2001**, *22*, 931; b) C. Fonseca Guerra, J.G. Snijders, G. te Velde, E.J. Baerends, *Theor. Chem. Acc.* **1998**, *99*, 391; c) ADF2019.102, SCM Theoretical Chemistry, Vrije Universiteit: Amsterdam (Netherlands). http://www.scm.com

Declaration by the candidate:

With regard to chapter 3 from pages 34–55, the nature and scope of my contribution were as follows:

Nature of contribution	Extent of contribution (%)
Conceptualization with other authors, Formal analysis, Investigation, Writing – Original Draft, Visualization.	45

The following co-authors have contributed to chapter 3 from pages 34–55:

Name	e-mail address	Nature of contribution	Extent of contribution(%)
Pascal Vermeeren	p.vermeeren@vu.nl	Formal analysis, Writing – Review & Editing, Supervision.	15
Marco Dalla Tiezza	marcodallatiezza@gmail.com	Formal analysis, Writing – Review & Editing, Supervision.	10
Catharine Esterhuysen	ce@sun.ac.za	Conceptualization, Formal analysis, Writing – Review & Editing, Supervision, Funding acquisition.	5
F. Matthias Bickelhaupt	f.m.bickelhaupt@vu.nl	Conceptualization, Formal analysis, Resources, Writing – Review & Editing, Supervision, Project administration, Funding acquisition.	10
Trevor A. Hamlin	t.a.hamlin@vu.nl	Conceptualization, Formal analysis, Writing – Review &	15

		Editing, Supervision, Project administration, Funding acquisition.	

Signature of candidate:……

Date:…23-11-2023…….

Declaration by co-authors:

The undersigned hereby confirm that

1. the declaration above accurately reflects the nature and extent of the contributions of the candidate and the co-authors to chapter 3 from pages 34–55,
2. no other authors contributed to chapter 3 from pages 34–55 besides those specified above, and
3. potential conflicts of interest have been revealed to all interested parties and that the necessary arrangements have been made to use the material in chapter 3 from pages 34–55 of this dissertation

Signature	Institutional affiliation	Date
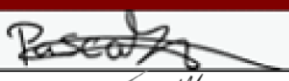	[1]	23-11-2023
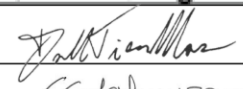	[1]	23 November 2023
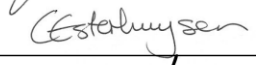	[2]	28 November 2023
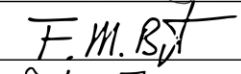	[1], [3], [4]	23 November 2023
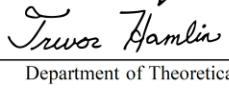	[1]	23 November 2023

[1] Department of Theoretical Chemistry, Amsterdam Institute of Molecular and Life Sciences (AIMMS), and Amsterdam Center for Multiscale Modeling (ACMM), Vrije Universiteit Amsterdam, De Boelelaan 1083, 1081 HV Amsterdam, The Netherlands

[2] Department of Chemistry and Polymer Science, Stellenbosch University, Private Bag X1, Matieland, Stellenbosch, 7602, South Africa

[3] Institute for Molecules and Materials (IMM), Radboud University, Heyendaalseweg 135, 6525 AJ Nijmegen, The Netherlands

[4] Department of Chemical Sciences, University of Johannesburg, Auckland Park, Johannesburg 2006, South Africa.

Chapter 3

Palladium-Catalyzed Activation of Carbon–Halogen Bonds: Electrostatics-Controlled Reactivity

Article Published in European Journal of Organic Chemistry

B.P. Moloto, P. Vermeeren, M. Dalla Tiezza,
C. Esterhuysen, F.M. Bickelhaupt, T.A. Hamlin

Eur. J. Org. Chem. **2022**, 184–190.

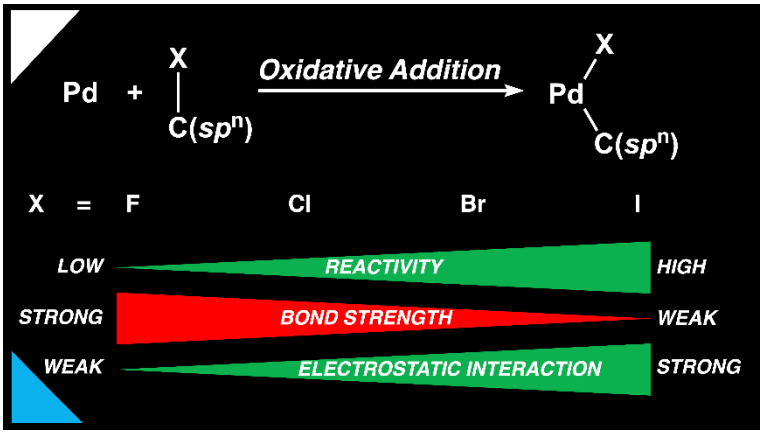

We have quantum chemically studied the palladium-mediated activation of C(sp^n)–X bonds (n = 1–3; X = F, Cl, Br, I) in the archetypal model substrates $H_3C–CH_2–X$, $H_2C=CH–X$, and HC≡C–X by a model bare palladium catalyst, using relativistic density functional theory at ZORA-BLYP/TZ2P. The bond activation reaction barrier decreases, for all *sp*-hybridized carbon centers, when the substituent X of the substrate is changed from X = F to I. Activation strain and energy decomposition analyses reveal that the enhanced reactivity along this series originates from (i) a less destabilizing activation strain due to an intrinsically weaker C(sp^n)–X bond; and (ii) an increasingly more stabilizing electrostatic interaction between the catalyst and the substrate. The latter is a direct consequence of the more diffuse electron density and higher nuclear charge of the X atom in the C(sp^n)–X bond when going from X = F to I, which, in turn, engages in a more favorable electrostatic attraction with the nucleus and electrons, respectively, of the palladium catalyst.

3.1 Introduction

Transition metal catalysis plays a key role in many industrial processes, as well as in the synthesis of various biologically active compounds.[1] An important class of catalytic processes is constituted by palladium-catalyzed cross-coupling reactions which furnish new carbon–carbon bonds (Scheme 3.1).[2] The first and, commonly, the rate-determining step in the catalytic cycle of this archetypical cross-coupling reaction is the activation of a carbon–element bond (C(sp^n)–X) by oxidative addition to the palladium center of the catalyst.[3] This reaction step plays an essential role in the selectivity and efficiency of the overall catalytic cycle. The oxidative addition is followed by a transmetalation step, whereby substituent A on the palladium metal center is replaced by hydrocarbon R. In the last step, the original palladium catalyst is regenerated by a reductive elimination step (the reverse of oxidative addition), yielding the new C(sp^n)–R bond. In a typical homogenous catalytic reaction, as mentioned earlier, the oxidative addition step is rate-limiting, and as such, has been the focus of extensive experimental[4] and theoretical studies.[5,6] Considering the importance of oxidative addition, a deep understanding of the underlying mechanism is crucial to designing new catalysts and improving the existing ones.

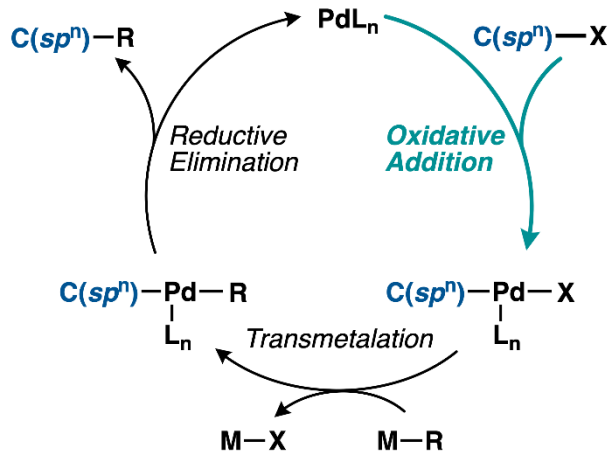

Scheme 3.1. Schematic catalytic cycle of a palladium-catalyzed cross-coupling reaction.

To understand the effect of varying the substituent X of C(sp^n)–X (n = 1–3; X = F, Cl, Br, I) in the bond activation process, we have quantum chemically explored the potential energy surface (PES) of the oxidative addition reaction of C(sp^n)–X by a model bare Pd catalyst, using relativistic density functional theory at ZORA-BLYP/TZ2P (Scheme 3.2). To this end, we have chosen to represent common motifs of reactants in palladium-catalyzed reactions through archetypal model C(sp^n)–X substrates, with C(sp^n) = $H_3C–CH_2–$ (sp^3), $H_2C=CH–$ (sp^2),

HC≡C– (*sp*). Recently, we have found that key reactivity trends are already nicely captured with bare Pd and that the addition of ligands to the catalyst results, independent of the nature of the C–X bond that is being activated, in an increase of the activation energy.[6] The activation strain model (ASM)[7] in combination with quantitative Kohn–Sham molecular orbital (KS-MO) theory[8] and a matching energy decomposition analysis (EDA) scheme[9] were employed to unravel the trends in reactivity and provide quantitative insights into the effect of variating the substituent X on the C(sp^n)–X bond activation. This computational methodology provides deep physical insight into the factors controlling reactivity and has proven useful for the understanding of, among others, oxidative addition reactions.[6]

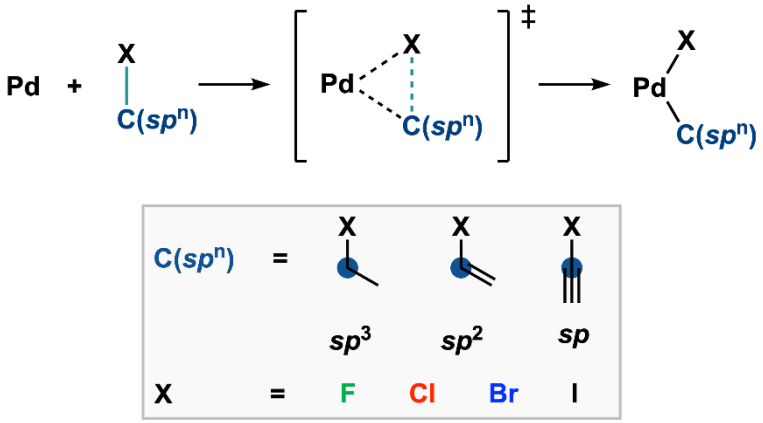

Scheme 3.2. Model oxidative addition reactions between Pd and C(sp^n)–X, where C(sp^n) = $H_3C–CH_2–$ (sp^3), $H_2C=CH–$ (sp^2), HC≡C– (*sp*); and X = F, Cl, Br, I.

3.2 Computational Methods

Computational Details

All calculations were executed with the Amsterdam Density Functional (ADF) program.[10] The generalized gradient approximation (GGA) functional BLYP[11] was used for the optimizations of all stationary points and subsequent analyses. The basis set used, denoted TZ2P,[12] is of triple-ζ quality and is augmented with two sets of polarization functions on each atom. Scalar relativistic effects were taken into account using the zeroth-order regular approximation (ZORA).[13] This level of theory is denoted as ZORA-BLYP/TZ2P and has been widely tested with several *ab initio* reference benchmarks up until the coupled cluster CCSD(T).[14] The accuracies of the fit schemes (Zlm fit for all computations except the decomposition of the electrostatic interaction term as shown in Eq. 3 below, which, for

technical reasons, was performed with the STO fitting scheme [15a]) and integration grid (Becke grid) were set to VERYGOOD.[15b,15c] Through vibrational analysis, all stationary points were confirmed to be either equilibrium structures (zero imaginary frequencies) or transition states (one single imaginary frequency).[16] Furthermore, the normal mode character associated with the imaginary frequency was analyzed to ensure that the correct transition state was found. The potential energy surfaces (PESs) of the studied oxidative addition reactions were obtained by utilizing intrinsic reaction coordinate (IRC) calculations.[17] The obtained PESs were further analyzed using the PyFrag 2019 program.[18] All stationary-point structures were illustrated using CYLview.[19]

Activation Strain Model and Energy Decomposition Analysis

The activation strain model (ASM,[7] also known as the distortion/interaction model[20]) is a fragment-based approach to understand the energy profile of a chemical process in terms of the original reactants, which are the model bare palladium catalyst and the substrate C(sp^n)–X. It considers their rigidity and the extent to which the reactants must deform during the reaction plus their capability to interact as the reaction proceeds. In this model, we decompose the total energy, $\Delta E(\zeta)$, into the strain and interaction energy, $\Delta E_{strain}(\zeta)$ and $\Delta E_{int}(\zeta)$, respectively, along the IRC which is projected onto a reaction coordinate ζ that is critically involved in the reaction [Eq. (3.1)].

$$\Delta E(\zeta) = \Delta E_{strain}(\zeta) + \Delta E_{int}(\zeta) \quad (3.1)$$

In this equation, the strain energy, $\Delta E_{strain}(\zeta)$, is the energy required to deform the reactants from their equilibrium structure to the geometry they acquire during the reaction at an arbitrary point ζ of the reaction coordinate. On the other hand, the interaction energy, $\Delta E_{int}(\zeta)$, accounts for all the mutual interactions that occur between the deformed fragments along the reaction coordinate.

The interaction energy between the deformed reactants is further analyzed with the help of our canonical energy decomposition analysis (EDA) scheme.[9] The EDA decomposes the $\Delta E_{int}(\zeta)$ into the following three energy terms [Eq. (3.2)]:

$$\Delta E_{int}(\zeta) = \Delta V_{elstat}(\zeta) + \Delta E_{Pauli}(\zeta) + \Delta E_{oi}(\zeta) \quad (3.2)$$

From this equation, $\Delta V_{\text{elstat}}(\zeta)$ is the quasi-classical electrostatic interaction between the unperturbed charge distributions of the deformed reactants. The $\Delta V_{\text{elstat}}(\zeta)$ can be further divided into four components [Eq. (3.3)]:

$$\Delta V_{\text{elstat}} = \sum_{\substack{\alpha \epsilon A \\ \beta \epsilon B}} \frac{Z_\alpha Z_\beta}{R_{\alpha\beta}} - \int \sum_{\alpha \epsilon A} \frac{Z_\alpha \rho^B(r)}{|R_\alpha - r|} \mathrm{d}r - \int \sum_{\beta \epsilon B} \frac{Z_\beta \rho^A(r)}{|R_\beta - r|} \mathrm{d}r + \int \int \frac{\rho^A(r_1)\rho^B(r_2)}{r_{12}} \mathrm{d}r_1 \mathrm{d}r_2 \quad (3.3)$$

Where A and B stand for the catalyst Pd and the substrate C(sp^n)–X. The first term is the electrostatic repulsion between the nuclei of fragments A and B. The second and third terms are the electrostatic attraction between the nuclei of fragment A and the electron density of fragment B and vice versa; while the last term is the electrostatic repulsion between the electron densities of fragments A and B.

The Pauli repulsion, $\Delta E_{\text{Pauli}}(\zeta)$, emerges from the destabilizing interaction between occupied orbitals (more precisely, electrons of same spin) on either of the fragments due to Pauli's exclusion principle. Lastly, the orbital interaction energy, $\Delta E_{\text{oi}}(\zeta)$, accounts for charge transfer (*e.g.,* HOMO–LUMO interactions) and polarization between the fragments. A detailed, step-by-step guide on how to perform and interpret the ASM and EDA can be found in Ref. [7c].

In this work, the activation strain and energy decomposition analyses were carried out along the intrinsic reaction coordinate (IRC) projected onto the stretch of the activated C(sp^n)•••X bond which is a critical geometry parameter of the reaction.[21] This particular geometric parameter undergoes a well-defined change during the reaction going from the reactant complex via the transition state to the product complex and has been shown to be a useful reaction coordinate for studying oxidative addition reactions.[6]

Thermochemistry

The bond dissociation energies (BDE), also known as bond enthalpies (ΔH_{BDE}), are calculated at normal temperature and pressure (NTP, *i.e.*, 298.15 K and 1 atm) from electronic bond energies (ΔE) and vibrational frequencies using the canonical thermochemistry relations for an ideal gas [Eq. (3.4)].[22]

$$\Delta H_{\text{BDE}} = \Delta E + \Delta E_{\text{trans,298.15}} + \Delta E_{\text{rot,298.15}} + \Delta E_{\text{vib,0}} + \Delta(\Delta E_{\text{vib,0}})_{298.15} \quad (3.4)$$

Herein, $\Delta E_{trans,298.15}$, $\Delta E_{rot,298.15}$, and $\Delta E_{vib,0}$ are the differences in translational, rotational, and zero-point vibrational energy between the C(sp^n)–X substrate and the homolytically dissociated fragments, C(sp^n)$^\bullet$ and X$^\bullet$ radical. The last term, $\Delta(\Delta E_{vib,0})_{298.15}$, is the vibrational correction energy to bring the system from 0 K to 298.15 K.

3.3 Results and Discussion

The substrates investigated in this work follow the series C(sp^n)–X; where C(sp^n) = $H_3C–CH_2–$ (sp^3), $H_2C=CH–$ (sp^2), HC≡C– (sp) and X = F, Cl, Br, I. We begin by first discussing the bond lengths and strengths of these C(sp^n)–X bonds in the substrates, which is a critical aspect of the overall bond activation process (*vide infra*). Table 3.1 contains the computed bond lengths and bond dissociation enthalpies at ZORA-BLYP/TZ2P. Two primary trends emerge, first the C(sp^n)–X bond becomes, for all *sp*-hybridized carbon atom centers, weaker and longer as X varies from F to I. For example, along the $H_2C=CH–X$ (sp^2) series, the bond strength and length go from 129.5 kcal mol^{-1} and 1.370 Å for $H_2C=CH–F$ to 65.0 kcal mol^{-1} and 2.131 Å for $H_2C=CH–I$. Blokker *et al.* have shown that this trend in bond strength on going down Group

Table 3.1. C(sp^n)–X bond lengths (in Å) and bond dissociation enthalpies (in kcal mol^{-1}), where C(sp^n) = $H_3C–CH_2–$ (sp^3), $H_2C=CH–$ (sp^2), HC≡C– (sp); and X = F, Cl, Br, I.[a]

Substrate	Bond type	C(sp^n)–X	ΔH_{BDE}
$H_3C–CH_2–F$	C(sp^3)–F	1.426	117.7
$H_3C–CH_2–Cl$	C(sp^3)–Cl	1.842	79.5
$H_3C–CH_2–Br$	C(sp^3)–Br	2.013	67.9
$H_3C–CH_2–I$	C(sp^3)–I	2.220	55.6
$H_2C=CH–F$	C(sp^2)–F	1.370	129.5
$H_2C=CH–Cl$	C(sp^2)–Cl	1.762	90.2
$H_2C=CH–Br$	C(sp^2)–Br	1.929	77.6
$H_2C=CH–I$	C(sp^2)–I	2.131	65.0
HC≡C–F	C(sp)–F	1.294	137.3
HC≡C–Cl	C(sp)–Cl	1.650	108.2
HC≡C–Br	C(sp)–Br	1.812	95.6
HC≡C–I	C(sp)–I	2.010	86.2

[a] Computed at ZORA-BLYP/TZ2P (enthalpies at 298.15 K and 1 atm).

17 does not originate from the decreasing electronegativity difference, but, instead, due to the increasing Pauli repulsion across the C(sp^n)–X bond for the larger halogen atoms.[23] Second, the C(sp^n)–X bond becomes stronger, and shorter when the *sp*-hybridization of the carbon center changes from sp^3 to sp^2 to *sp*, while keeping the substituent X constant, *e.g.*, from 117.7 kcal mol^{-1} and 1.426 Å for $H_3C–CH_2–F$ to 137.3 kcal mol^{-1} and 1.294 Å for HC≡C–F. Recently, we have shown that the underlying physical mechanism behind this structural trend is the reduction of steric congestion around the C(sp^n) atom, that is, the reduction in the destabilizing Pauli repulsion between the C(sp^n) fragment and the substituent X as the number of substituents around the pertinent C(sp^n) atom goes down from 4, to 3, to 2, along sp^3 to sp^2 to *sp* hybridization.[24]

The results of our computed ZORA-BLYP/TZ2P reaction profiles for the studied C(sp^n)–X bond activation reactions are collected in Table 3.2 and Figures 3.1 and S3.1 The reactions proceed via a reactant complex (RC) and a transition state (TS), towards the product complex (PC).

Table 3.2. Energies relative to reactants (in kcal mol^{-1}) of the stationary points for the oxidative addition of Pd into the C(sp^n)–X bond (X = F, Cl, Br, I).[a,b]

Substrate	Bond type	RC	TS	PC
$H_3C–CH_2–F$	C(sp^3)–F	–5.5	17.6	–13.7
$H_3C–CH_2–Cl$	C(sp^3)–Cl	–13.5	–0.9	–32.5
$H_3C–CH_2–Br$	C(sp^3)–Br	–17.0	–6.4	–37.3
$H_3C–CH_2–I$	C(sp^3)–I	–22.8	–12.5	–41.7
$H_2C=CH–F$	C(sp^2)–F	–31.6	5.3	–13.5
$H_2C=CH–Cl$	C(sp^2)–Cl	–31.8	–15.9	–33.4
$H_2C=CH–Br$	C(sp^2)–Br	–32.8	–22.8	–39.5
$H_2C=CH–I$	C(sp^2)–I	–33.4	–28.5	–44.5
HC≡C–F	C(*sp*)–F	–38.2	0.1	–24.2
HC≡C–Cl	C(*sp*)–Cl	–35.2	–17.5	–35.1
HC≡C–Br	C(*sp*)–Br	–36.4	–24.6	–41.9
HC≡C–I	C(*sp*)–I	–36.3	–28.4	–45.3

[a] Computed at ZORA-BLYP/TZ2P. [b] See Figures 1 and S3.1 for stationary-point structures.

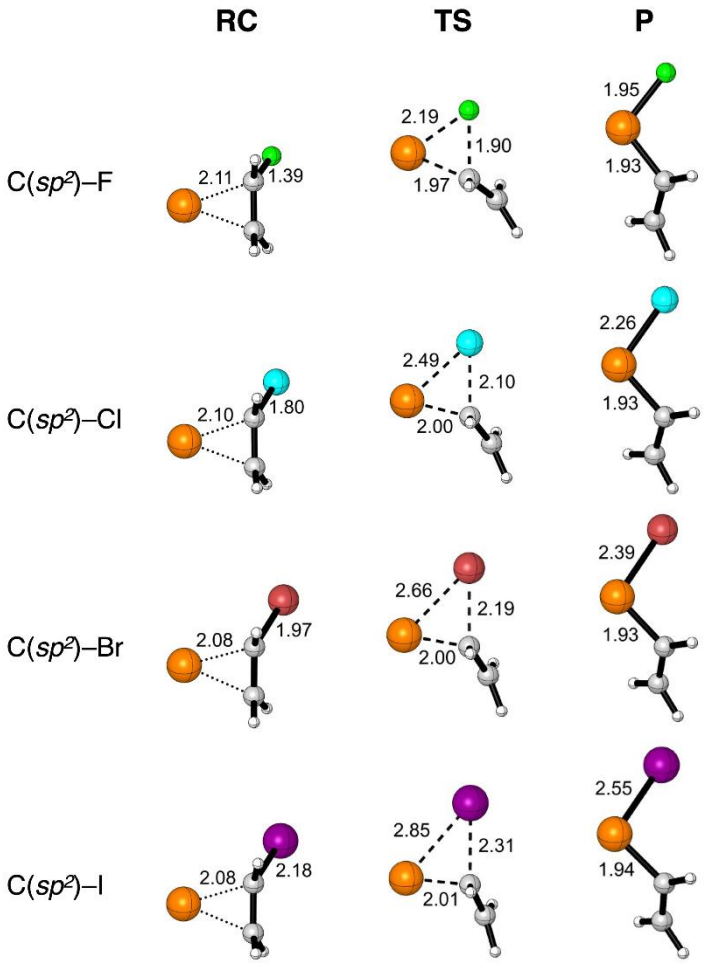

Figure 3.1. Stationary-point structures (in Å) for the oxidative addition of Pd into the C(sp^2)–X bond (X = F, Cl, Br, I), computed at ZORA-BLYP/TZ2P. Atoms colors: H = white, C = gray, F = green, Cl = cyan, Br, = brown, I = purple, Pd = orange.

Note, that the overall activation energy $\Delta E^{\ddagger}$, that is, the energy difference between the TS and the infinitely separated reactants (Pd and C(sp^n)–X), can be negative if a substantially stabilized reactant complex is formed. For a more detailed discussion on the various types of reaction potential energy surfaces, see, for example, Reference 25. Based on the reaction profiles, two distinct reactivity trends can be discerned from this data. First, the overall activation energy for the oxidative addition process decreases, for all *sp*-hybridized substrates, upon going down in Group 17 from X = F to I, *e.g.*, the activation energy goes down from 5.3 kcal mol^{-1} for H_2C=CH–F to –28.5 kcal mol^{-1} for H_2C=CH–I. Second, changing the *sp*-hybridization of the carbon atom constituting the C(sp^n)–X bond from sp^3 to sp^2 to *sp* while keeping the substituent X constant leads, in general, to a lowering of the reaction barrier. For example, for C(sp^n)–F, the reaction barrier goes from 17.6 kcal mol^{-1} for H_3C–CH_2–F to 0.1 kcal mol^{-1} for HC≡C–F. There is, however, one exception, namely, HC≡C–I has a slightly higher reaction barrier than H_2C=CH–I (–28.4 kcal mol^{-1} *versus* –28.5 kcal mol^{-1}, respectively).

The latter reactivity trend, that is what happens when one varies the *sp*-hybridization of the carbon atom of C(sp^n)–X bond from sp^3 to sp^2 to *sp* while keeping the substituent X constant has recently been studied by our group.[26] We have found that the reaction barrier decreases along C(sp^3)–X to C(sp^2)–X to C(*sp*)–X, even though the bond becomes substantially stronger and hence requires consistently more energy to break during the oxidative addition process. This reactivity trend is, in fact, established by the reduction of Pauli repulsion between the Pd catalyst and the substrate. Going from C(sp^3)–X to C(sp^2)–X to C(*sp*)–X, the number of substituents around the pertinent carbon atom goes down from 4 to 3 to 2, causing less steric interactions between occupied orbitals of the Pd catalyst and the occupied orbitals with amplitude on the substituents of the substrate. The reactivity trend becomes reinforced by an increasingly more stabilizing π-backbonding interaction, which is the result of a smaller catalyst–substrate HOMO–LUMO gap between the d_π and $\sigma^*_{C(spn)–X}$ orbitals, as the orbital energy of the substrate $\sigma^*_{C(spn)–X}$ orbital drops along sp^3 to sp^2 to *sp*.[24]

To gain quantitative insight into the physical factors governing the bond activation trend when changing the substituent X, we applied the activation strain model (ASM) of chemical reactivity.[7] Figure 3.2 shows the activation strain diagrams (ASDs) of the C(sp^2)–X bond activation by the model bare Pd catalyst along the IRC are projected on the C(sp^2)•••X bond stretch (see the Computational Methods for more details). The ASDs of all other substrates, *i.e.*, C(sp^3)–X and C(*sp*)–X, possess the same features and are provided in Figures S3.2 and S3.3 of the Supporting Information. As found in Table 3.2, the reaction barrier goes down from C(sp^2)–F to C(sp^2)–I, which can be traced back to both a less destabilizing strain energy and a more stabilizing interaction energy along this series (Figures 3.2b and 3.2c). The trend in strain energy originates from the increasingly weaker, and longer, C(sp^2)–X bond going from X = F to I (*vide supra*; Table 3.1). The weaker the C(sp^2)–X bond, the easier it becomes to break, and hence it generates less activation strain during the oxidative addition process.

Next, we turn to the energy decomposition analysis (EDA) to get a better understanding of why the interaction energy becomes more stabilizing from C(sp^2)–F to C(sp^2)–I. Interestingly, and in contrast to our previous studies on palladium-mediated bond activation trends,[6] the enhanced interaction energy upon going from C(sp^2)–F to C(sp^2)–I is exclusively determined by the electrostatic interaction (Figure 3.2d).

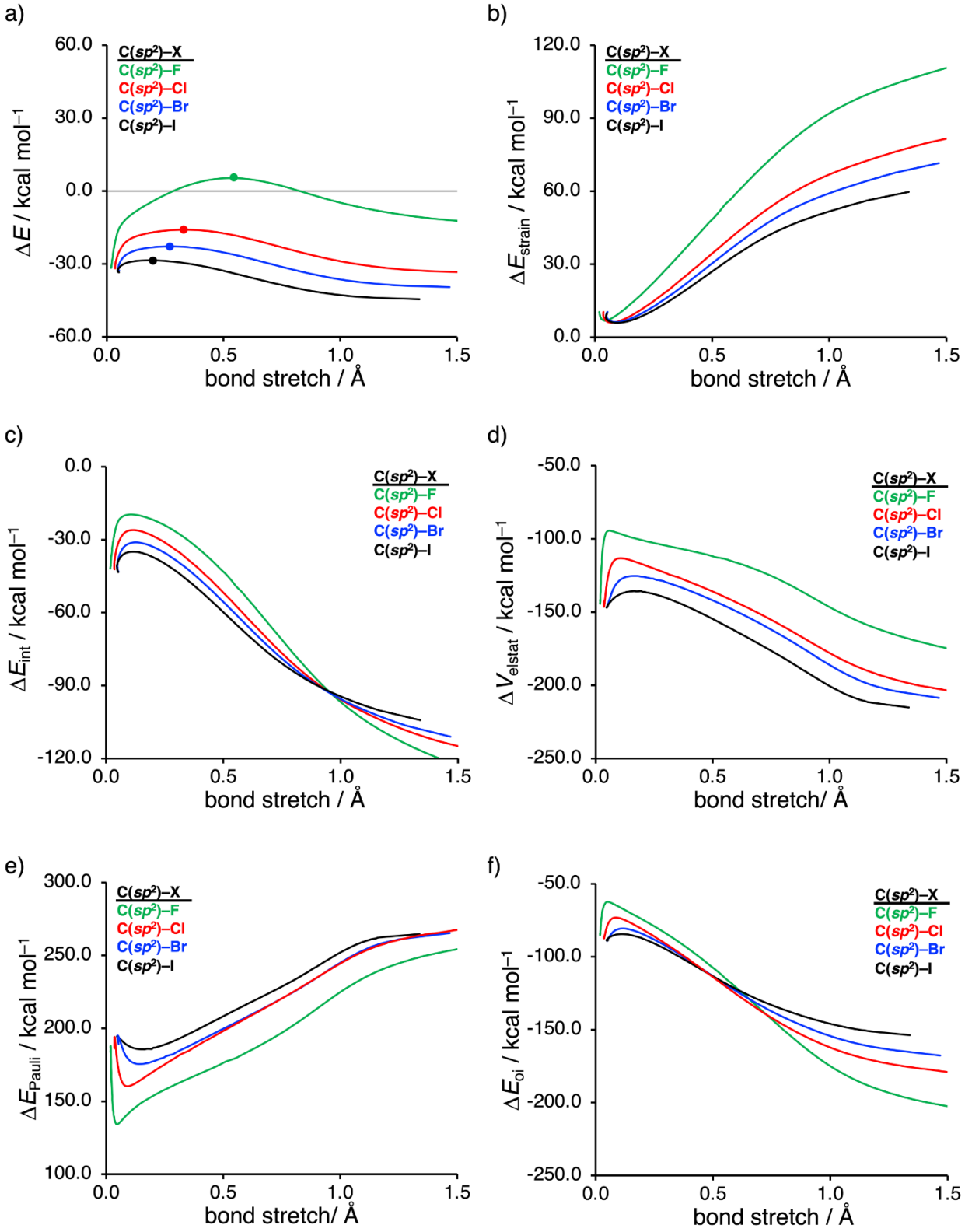

Figure 3.2. Activation strain analyses: a) total energy, b) strain energy, c) interaction energy; and energy decomposition analyses: d) electrostatic interaction, e) Pauli repulsion, and f) orbital interactions, for the oxidative addition of Pd into the C(sp^2)–X bond (X = F, Cl, Br, I), where the transition states are indicated with a dot and the energy terms along the IRC are projected on the C(sp^2)•••X bond stretch. Computed at ZORA-BLYP/TZ2P.

The least stabilizing electrostatic interaction is found for the Pd insertion into the C(sp^2)–F bond and this effect becomes increasingly more stabilizing when going down Group 17 for atom X in C(sp^2)–X. The Pauli repulsion and orbital interactions (Figures 3.2e and 3.2f), on the other hand, are significantly less important or show even an opposite trend.

Finally, to get a more detailed insight into the origin of the reactivity trend, we decompose the electrostatic interaction into the repulsive and attractive electrostatic contributions according to Equation 3.3 at consistent geometries obtained from the IRC with a C(sp^2)•••X bond stretch of 0.335 Å (Table 3.3, see Tables S3.2 and S3.3 for other substrates). Performing this analysis at a consistent point along the reaction coordinate (near all transition state structures), rather than on the individual transition state structures alone, ensures that the results are not skewed by the position, earlier or later, of the transition state.[7b] As seen in Figure 3.2d, the electrostatic interactions become more stabilizing upon going down in Group 17 for substituent X, namely, from –114.0 kcal mol^{-1} for C(sp^2)–F to –155.0 kcal mol^{-1} for C(sp^2)–I. This trend of consistently more stabilizing electrostatic interactions is exclusively determined by the attractive electrostatic interaction, *i.e.*, the $\text{nuclear}_{\text{Pd}}$–$\text{electron}_{\text{C}(sp2)–\text{X}}$ and $\text{electron}_{\text{Pd}}$–$\text{nuclear}_{\text{C}(sp2)–\text{X}}$ attraction.

Table 3.3 Decomposition of the Pd–substrate electrostatic interactions (in kcal mol^{-1}) for the oxidative addition of Pd into the C(sp^2)–X bond (X = F, Cl, Br, I).[a,b]

Substrate	Repulsive electrostatic interactions[c]	Attractive electrostatic interactions[d]	Total electrostatic interactions
C(sp^2)–F	311,806.4	–311,920.4	–114.0
C(sp^2)–Cl	398,457.3	–398,596.2	–138.9
C(sp^2)–Br	597,485.0	–597,632.6	–147.7
C(sp^2)–I	775,514.0	–775,669.0	–155.0

[a] Analyses at consistent geometries obtained from the IRC with a C(sp^2)•••X bond stretch of 0.335 Å at ZORA-BLYP/TZ2P. [b] The interacting reactants are the bare palladium model catalyst and the substrate C(sp^2)–X. [c] Repulsive electrostatic interactions are the sum of the $\text{nuclear}_{\text{Pd}}$–$\text{nuclear}_{\text{C}(sp2)–\text{X}}$ and $\text{electron}_{\text{Pd}}$–$\text{electron}_{\text{C}(sp2)–\text{X}}$ repulsion. [d] Attractive electrostatic interactions are the sum of the $\text{nuclear}_{\text{Pd}}$–$\text{electron}_{\text{C}(sp2)–\text{X}}$ and $\text{electron}_{\text{Pd}}$–$\text{nuclear}_{\text{C}(sp2)–\text{X}}$ attraction.

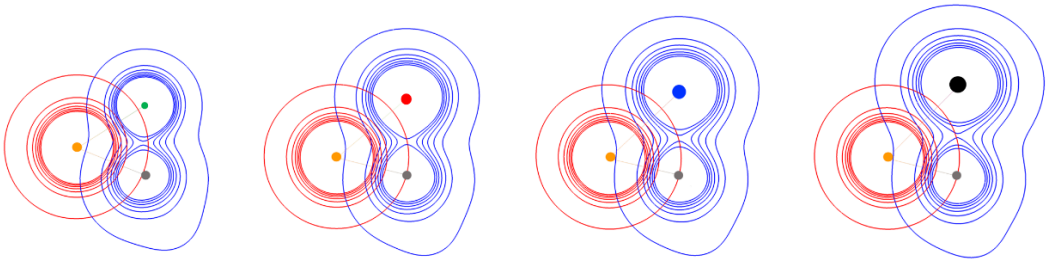

	C(sp^2)–F	C(sp^2)–Cl	C(sp^2)–Br	C(sp^2)–I
r C(sp^2)•••Pd	1.978	2.001	1.993	1.993
r X•••Pd	2.243	2.493	2.638	2.779

Figure 3.3 Density contours from –0.095 to 0.099 Bohr^{-3} for the oxidative addition of Pd into the C(sp^2)–X bond (X = F, Cl, Br, I; electron density of Pd in red; electron density of C(sp^2)–X substrate in blue; distances in Å) at consistent geometries along the IRC with a C(sp^2)•••X bond stretch of 0.335 Å, computed at ZORA-BLYP/TZ2P. Atom colors: C = gray, F = green, Cl = red, Br, = blue, I = black, Pd = orange.

The attractive electrostatic interactions between Pd and C(sp^2)–X become more stabilizing from X = F to I, due to (i) a more diffuse electron density; and (ii) a higher nuclear charge of the larger atom X. In Figure 3.3, we plot the electron density of the palladium catalyst (red) and C(sp^2)–X (blue) at consistent geometries obtained from the IRC with a C(sp^2)•••X bond stretch of 0.335 Å (see Figures S3.4 and S3.5 for other substrates). When going down Group 17, the electron density on atom X naturally increases and expands and hence overlaps better with the nucleus of the Pd catalyst, even though the distance between X•••Pd increases from 2.243 Å for X = F to 2.779 Å for X = I, resulting in a more favorable nuclear$_{Pd}$–electron$_{C(sp2)–X}$ attraction. In addition, the nuclear charge on atom X also increases along the studied series from $Z_{C(sp2)–X}$ = 9 for C(sp^2)–F to $Z_{C(sp2)–X}$ = 53 for C(sp^2)–I, leading to a more attractive electron$_{Pd}$–nuclear$_{C(sp2)–X}$ interaction upon going down in Group 17. These two enhanced electrostatic attractions, ultimately, result in the more stabilizing interaction energy and hence a lower reaction barrier for the bond activation of C(sp^2)–F compared to C(sp^2)–I by the palladium catalyst. The repulsive electrostatic interactions, on the other hand, become more destabilizing from C(sp^2)–F to C(sp^2)–I and, therefore, partly but not completely, counteract the trend dictated by the attractive electrostatic interactions. Interestingly, a similarly decisive role, and mechanism, of electrostatic interactions was found before in a quite different context, namely, in the trend in the preferred conformation of α-halocarbonyl compounds.[27]

3.4. Conclusions

Our computational study quantifies the reactivity trends of the oxidative addition reaction between Pd and C(sp^n)–X (n = 1–3 and = F, Cl, Br, I) in archetypal model substrates H_3C–CH_2–X (sp^3), H_2C=CH–X (sp^2), and HC≡C–X (sp), using relativistic density functional theory. We have found that the reaction barrier of C(sp^n)–X bond activation systematically decreases, for all sp^n-hybridized carbon atoms along the series C(sp^n)–F > C(sp^n)–Cl > C(sp^n)–Br > C(sp^n)–I.

Our activation strain and energy decomposition analyses reveal that the decreased oxidation addition reaction barrier of C(sp^n)–X by Pd going down Group 17 from X = F to Cl to Br to I originates from two factors: (i) a less destabilizing activation strain; and (ii) a more favorable electrostatic attraction between the catalyst and the substrate. Going down Group 17, the C(sp^n)–X bond becomes weaker, as explained by Blokker *et al.*[23] The weaker the bond, the easier it is to break and hence the less activation strain it generates during the oxidative addition reaction.

The electrostatic interaction between the catalyst and substrate also becomes more favorable when changing the substrate from C(sp^n)–F to C(sp^n)–I. The larger X atom has a more diffuse and electron-rich density and a higher nuclear charge, which, in turn, can engage in more favorable electrostatic attraction with the palladium nucleus and electron density, respectively. This effect makes the oxidative addition reaction involving the C(sp^n)–X bond with a larger X atom correspond to a more stabilizing interaction and hence lower reaction barrier. These findings will equip experimentalists with the mechanistic insight to understand and predict the trends in reactivity of palladium-mediated oxidative addition reactions.

3.5. References

[1] a) J. Collman, L. Hegedus, J. Norton, R. Finke, *Principles and Applications of Organotransition Metal Chemistry*, **1987**; b) F. Diederich, P. J. Stang, *Metal-Catalyzed Cross-Coupling Reactions*, Wiley-VCH, Weinheim, **1998**; c) J. F. Hartwig, *Organotransition Metal Chemistry: From Bonding to Catalysis*, University Science Books, Sausalito, **2010**; d) P. W. N. M. van Leeuwen, *Homogeneous Catalysis: Understanding the Art*, Kluwer Academic Publishers, Dordrecht, **2004**; e) L. Souillart, N. Cramer, *Chem. Rev.* **2015**, *115*, 9410.

[2] a) C. C. C. Johansson Seechurn, M. O. Kitching, T. J. Colacot, V. Snieckus, *Angew. Chem. Int. Ed.* **2012**, *51*, 5062; b) E.-I. Negishi, *Angew. Chem. Int. Ed.* **2011**, *50*, 6738; c) A. Suzuki, *Angew. Chem. Int. Ed.* **2011**, *50*, 6722.

[3] a) G. B. Smith, G. C. Dezeny, D. L. Hughes, A. O. King, T. R. Verhoeven, *J. Org. Chem.* **1994**, *59*, 8151; b) Hydrogenation. In Homogeneous Catalysis, Springer Netherlands, Dordrecht, **2004**, pp. 75–100. c) B. Crociani, S. Antonaroli, L. Canovese, P. Uguagliati, F. Vizentin, *Eur. J. Inorg. Chem.* **2004**, 732; d) R. van Asselt, K. Vrieze, C. J. Elsevier, *J. Org. Chem.* **1994**, *480*, 27.

[4] a) J. C. Weisshaar, *Acc. Chem. Res.* **1993**, *26*, 213; b) A. E. Shilov, G. B. Shul'pin, *Chem. Rev.* **1997**, *97*, 2879; c) M. E. van der Boom, D. Milstein, *Chem. Rev.* **2003**, *103*, 1759; d) R. H. Crabtree, *J. Organomet. Chem.* **2004**, *689*, 4083; e) C.-H. Jun, *Chem. Soc. Rev.* **2004**, *33*, 610; f) M. Lersch, M. Tilset, *Chem. Rev.* **2005**, *105*, 2471; g) J. R. Hummel, J. A. Boerth, J. A. Ellman, *Chem. Rev.* **2016**, *117*, 9163.

[5] a) S. Niu, M. B. Hall, *Chem. Rev.* **2000**, *100*, 353; b) M. Torrent, M. Solà, G. Frenking, *Chem. Rev.* **2000**, *100*, 439; c) A. Dedieu, *Chem. Rev.* **2000**, *100*, 543; d) S. Kozuch, C. Amatore, A. Jutand, S. Shaik, *Organometallics* **2005**, *24*, 2319; e) L. Xue, Z. Lin, *Chem. Soc. Rev.* **2010**, *39*, 1692; f) D. Balcells, E. Clot, O. Eizenstein, *Chem. Rev.* **2010**, *110*, 749; g) M. Besora, C. Gourlaouen, B. Yates, F. Maseras, *Dalton Trans.* **2011**, *40*, 11089; h) M. Garcia-Melchor, A. A. Braga, A. Lledos, G. Ujaque, F. Maseras, *Acc. Chem. Res.* **2013**, *46*, 2626; i) J. Joy, T. Stuyver, S. Shaik, *J. Am. Chem. Soc.* **2020**, *142*, 3836.

[6] a) P. Vermeeren, X. Sun, F. M. Bickelhaupt, *Sci. Rep.* **2018**, *8*, 10729; b) L. P. Wolters, W.-J. van Zeist, F. M. Bickelhaupt, *Chem. Eur. J.* **2014**, *20*, 11370; c) L. P. Wolters, F. M. Bickelhaupt, *Chem. Asian J.* **2015**, *10*, 2272; d) X. Sun, T. Hansen, J. Poater, T. A. Hamlin, F. M. Bickelhaupt, *J. Comput. Chem.* **2022**, DOI: 10.1002/jcc.26818; e) T. Hansen, X. Sun, M. Dalla Tiezza, W. -J. van Zeist, J. N. P. van Stralen, D. P. Geerke, L. P. Wolters, T. A. Hamlin, F. M. Bickelhaupt, *Chem. Eur. J.* **2022**, e202201093.

[7] For reviews, see: a) F. M. Bickelhaupt, K. N. Houk, *Angew. Chem.* **2017**, *129*, 10204; *Angew. Chem. Int. Ed.* **2017**, *56*, 10070; b) P. Vermeeren, T. A. Hamlin, F. M. Bickelhaupt, *Chem Commun.* **2021**, *57*, 5880; For a step-by-step protocol, see: c) P. Vermeeren, S. C. C. van der Lubbe, C. Fonseca Guerra, F. M. Bickelhaupt, T. A. Hamlin, *Nat. Protoc.* **2020**, *15*, 649.

[8] a) R. van Meer, O. V. Gritsenko, E. J. Baerends, *J. Chem. Theory Comput.* **2014**, *10*, 4432; b) T. A. Albright, J. K. Burdett, M.-H. Whangbo, *Orbital Interactions in Chemistry*, John Wiley & Sons, Inc., **2013**.

[9] For an overview of the EDA method, see: a) T. A. Hamlin, P. Vermeeren, C. Fonseca Guerra, F. M. Bickelhaupt, in *Complementary Bonding Analysis*, (Ed. S. Grabowsky), De Gruyter, Berlin, **2021**, pp. 199–212; for a detailed overview of the EDA method, see: b) F. M. Bickelhaupt, E. J. Baerends, in *Reviews in Computational Chemistry*, (Eds. K. B. Lipkowitz, D. B. Boyd), Wiley, Hoboken, **2000**, pp. 1.

[10] a) G. te Velde, F. M. Bickelhaupt, E. J. Baerends, C. Fonseca Guerra, S. J. A. van Gisbergen, J. G. Snijders, T. Ziegler, *J. Comput. Chem.* **2001**, *22*, 931; b) C. Fonseca Guerra, J. G. Snijders, G. te Velde, E. J. Baerends, *Theor. Chem. Acc.* **1998**, *99*, 391; c) ADF2019.102, SCM Theoretical Chemistry, Vrije Universiteit: Amsterdam (Netherlands). http://www.scm.com.

[11] a) A. D. Becke, *Phys. Rev. A* **1988**, *38*, 3098; b) B. G. Johnson, P. M. W. Gill, J. A. Pople, *J. Chem. Phys.* **1993**, *98*, 5612; c) C. Lee, W. Yang, R. G. Parr, *Phys. Rev. B* **1988**, *37*, 785; d) T. V. Russo, R. L. Martin, P. J. Hay, *J. Chem. Phys.* **1994**, *101*, 7729.

[12] E. van Lenthe, E. J. Baerends, *J. Chem. Phys.* **2003**, *24*, 1142.

[13] a) E. van Lenthe, E. J. Baerends, J. G. Snijders, *J. Chem. Phys.* **1993**, *99*, 4597; b) E. van Lenthe, E. J. Baerends, J. G. Snijders, *J. Chem. Phys.* **1994**, *101*, 9783; c) E. van Lenthe, A. Ehlers, E. J. Baerends, *J. Chem. Phys.* **1999**, *110*, 8943.

[14] a) G. T. de Jong, M. Solà, L. Visscher, F. M. Bickelhaupt, *J. Chem. Phys.* **2004**, *121*, 9982; b) G. T. de Jong, D. P. Geerke, A. Diefenbach, F. M. Bickelhaupt, *J. Chem. Phys.* **2005**, *313*, 261; c) G. T. De Jong, D. P. Geerke, A. Diefenbach, M. Solà, F. M. Bickelhaupt, *J. Comput. Chem.* **2005**, *26*, 1006; d) G. Th. de Jong, F. M. Bickelhaupt, *J. Phys. Chem. A*, **2005**, *109*, 9685.

[15] a) E. J. Baerends, D. E. Ellis and P. Ros, *Chem. Phys.* **1973**, *2*, 41; b) M. Franchini, P. H. T. Philipsen, E. van Lenthe, L. Visscher, *J. Chem. Theory Comput.* **2014**, *10*, 1994; c) M. Franchini, P. H. T. Philipsen, L. Visscher, *J. Comput. Chem.* **2013**, *34*, 1819.

[16] a) A. Bérces, R. M. Dickson, L. Fan, H. Jacobsen, D. P. Swerhone, T. Ziegler, *Comput. Phys. Commun.* **1997**, *100*, 247; b) H. Jacobsen, A. Bérces, D. P. Swerhone, T. Ziegler, *Comput. Phys. Commun.* **1997**, *100*, 263; c) S. K. Wolff, *Int. J. Quantum Chem.* **2005**, *104*, 645.

[17] a) K. Fukui, *Acc. Chem. Res.* **1981**, *14*, 363; b) L. Deng, T. Ziegler, L. Fan, *J. Chem. Phys.* **1993**, *99*, 3823; c) L. Deng, T. Ziegler, *Int. J. Quantum Chem.* **1994**, *52*, 731.

[18] a) X. Sun, T. M. Soini, J. Poater, T. A. Hamlin, F. M. Bickelhaupt, *J. Comput. Chem.* **2019**, *40*, 2227; b) PyFrag 2019: X. Sun, T. Soini, L. P. Wolters, W.-J. van Zeist, C. Fonseca Guerra, T. A. Hamlin, F. M. Bickelhaupt, Vrije Universiteit Amsterdam, The Netherlands.

[19] CYLview2.0; C. Y. Legault, Université de Sherbrooke, 2020 (http://www.cylview.org).

[20] a) D. H. Ess, K. Houk, *J. Am. Chem. Soc.* **2007**, *129*, 10646; b) D. H. Ess, K. Houk, *J. Am. Chem. Soc.* **2008**, *130*, 10187.

[21] W.-J. van Zeist, A. H. Koers, L. P. Wolters, F. M. Bickelhaupt, *J. Chem. Theory Comput.* **2008**, *4*, 920.
[22] a) D. A. McQuarrie, J. D. Simon, Physical Chemistry: A Molecular Approach, University Science Books, Sausalito, Calif, **1997**; b) C. J. Cramer, Essentials of Computational Chemistry: Theories and Models, Wiley, Chichester, West Sussex, England; Hoboken, NJ, **2004**; c) F. Jensen, Introduction to Computational Chemistry, Wiley, Chichester, UK; Hoboken, NJ, **2017**; d) P. W. Atkins, J. De Paula, J. Keeler, Atkins' Physical Chemistry, Oxford University Press, Oxford, United Kingdom; New York, NY, **2018**.
[23] E. Blokker, X. Sun, J. Poater, J. M. van der Schuur, T. A. Hamlin, F. M. Bickelhaupt, *Chem. Eur. J.* **2021**, *27*, 15616.
[24] P. Vermeeren, W.-J. van Zeist, T. A. Hamlin, C. Fonseca Guerra, F. M. Bickelhaupt, *Chem. Eur. J.* **2021**, *27*, 7074.
[25] F. M. Bickelhaupt, *Mass Spectrom. Rev.* **2001** *20*, 347.
[26] T. Hansen, X. Sun, M. Dalla Tiezza, W. -J. van Zeist, J. Poater, T. A. Hamlin, F. M. Bickelhaupt, *Chem. Eur. J.* **2021**, e202103963.
[27] D. Rodrigues Silva, L. de Azevedo Santos, T. A. Hamlin, F. M. Bickelhaupt, M. P. Freitas, C. Fonseca Guerra, *Phys. Chem. Chem. Phys.* **2021**, *23*, 20883.

3.6. Supporting Information

Table S3.1. C(sp^n)–X bond lengths (in Å) in all the stationary-point structures for the oxidative addition of Pd into the C(sp^n)–X bond (X = F, Cl, Br, I).[a]

Substrate	Bond type	RC	TS	PC
$H_3C–CH_2–F$	C(sp^3)–F	1.423	1.819	3.038
$H_3C–CH_2–Cl$	C(sp^3)–Cl	1.886	2.123	3.299
$H_3C–CH_2–Br$	C(sp^3)–Br	2.065	2.266	3.395
$H_3C–CH_2–I$	C(sp^3)–I	2.263	2.449	3.540
$H_2C=CH–F$	C(sp^2)–F	1.388	1.904	3.055
$H_2C=CH–Cl$	C(sp^2)–Cl	1.796	2.095	3.305
$H_2C=CH–Br$	C(sp^2)–Br	1.973	2.191	3.383
$H_2C=CH–I$	C(sp^2)–I	2.182	2.314	3.482
HC≡C–F	C(sp)–F	1.328	1.816	2.972
HC≡C–Cl	C(sp)–Cl	1.698	1.923	3.136
HC≡C–Br	C(sp)–Br	1.869	1.993	3.193
HC≡C–I	C(sp)–I	2.071	2.147	3.249

[a] Computed at ZORA-BLYP/TZ2P.

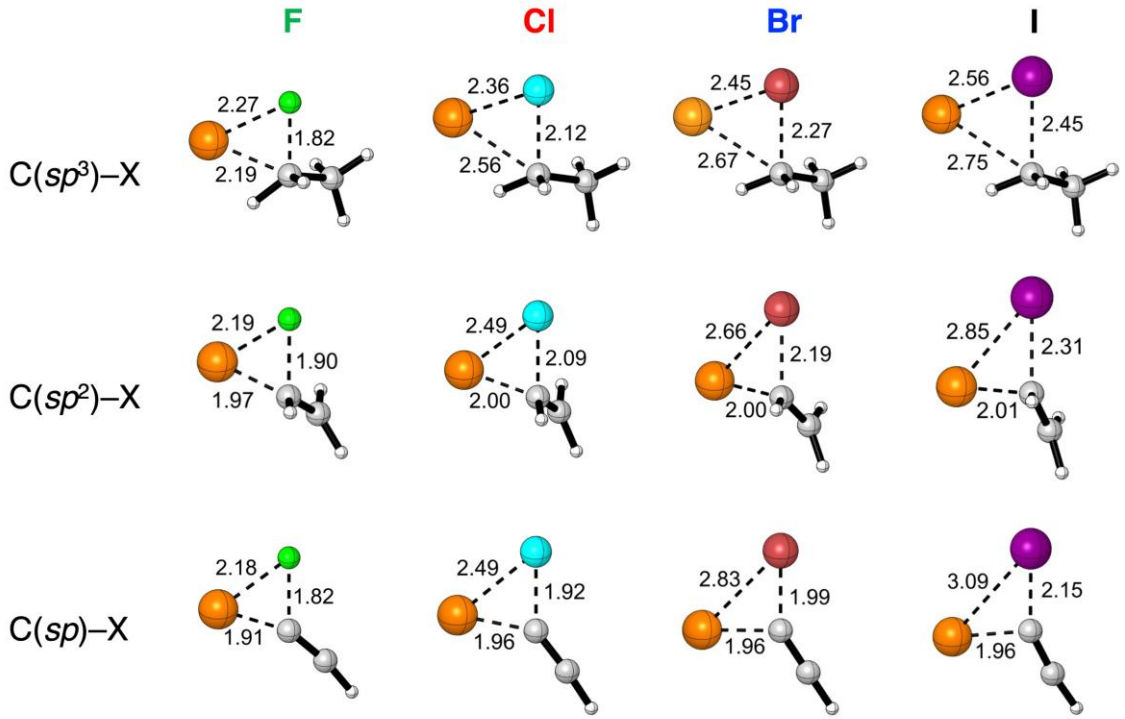

Figure S3.1. Transition state structures (in Å) for the oxidative addition of Pd into the C(sp^n)–X bond (n = 1, 2, 3; and X = F, Cl, Br, I), computed at ZORA-BLYP/TZ2P. H = white, C = gray, F = green, Cl = cyan, Br, = brown, I = purple, Pd = orange.

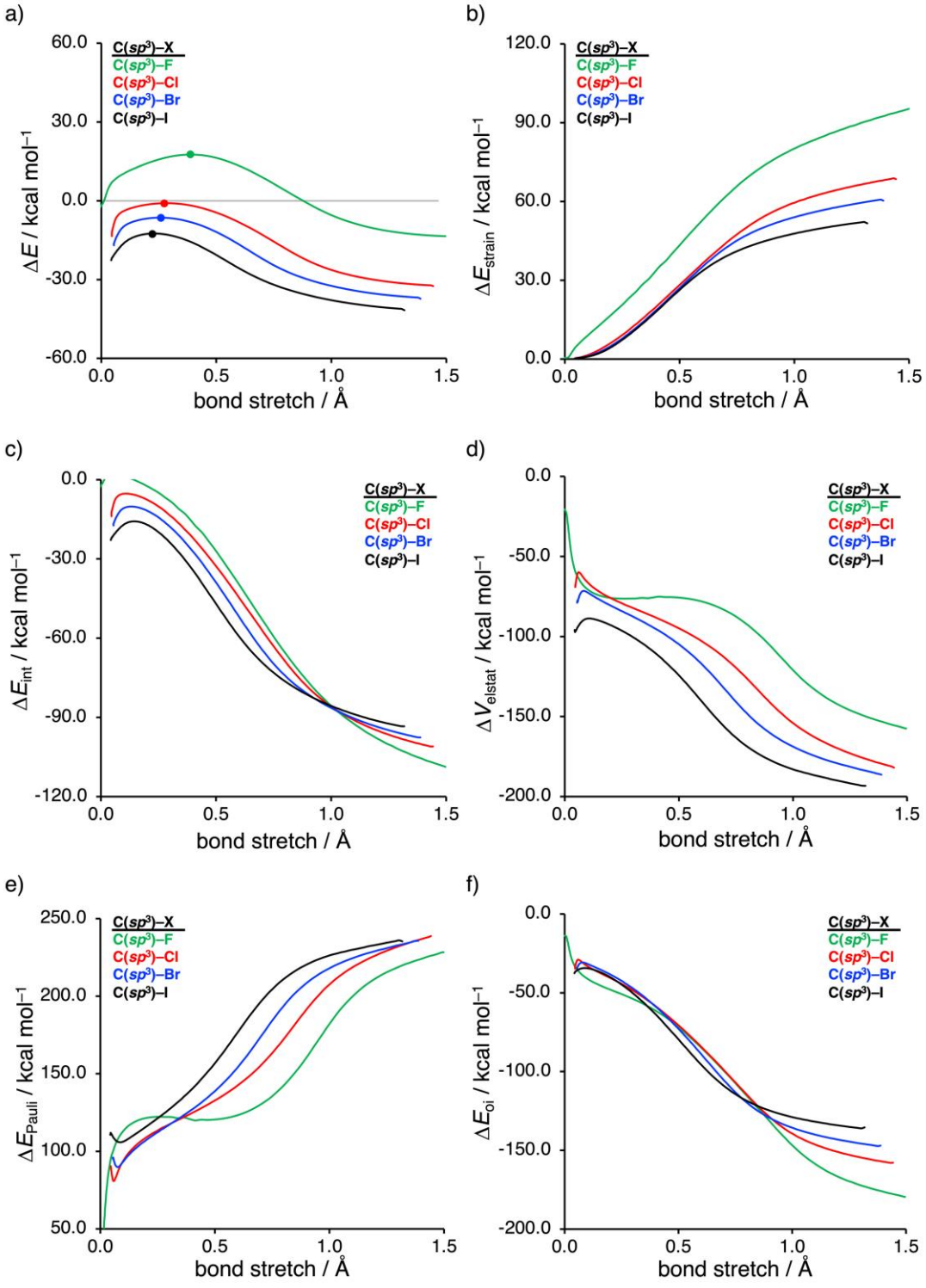

Figure S3.2. Activation strain analyses: a) total energy, b) strain energy, c) interaction energy; and energy decomposition analyses: d) electrostatic interaction, e) Pauli repulsion, and f) orbital interactions, for the oxidative addition of Pd into the C(sp^3)–X bond (X = F, Cl, Br, I), where the transition states are indicated with a dot and the energy terms along the IRC are projected on the C(sp^3)•••X bond stretch. Computed at ZORA-BLYP/TZ2P.

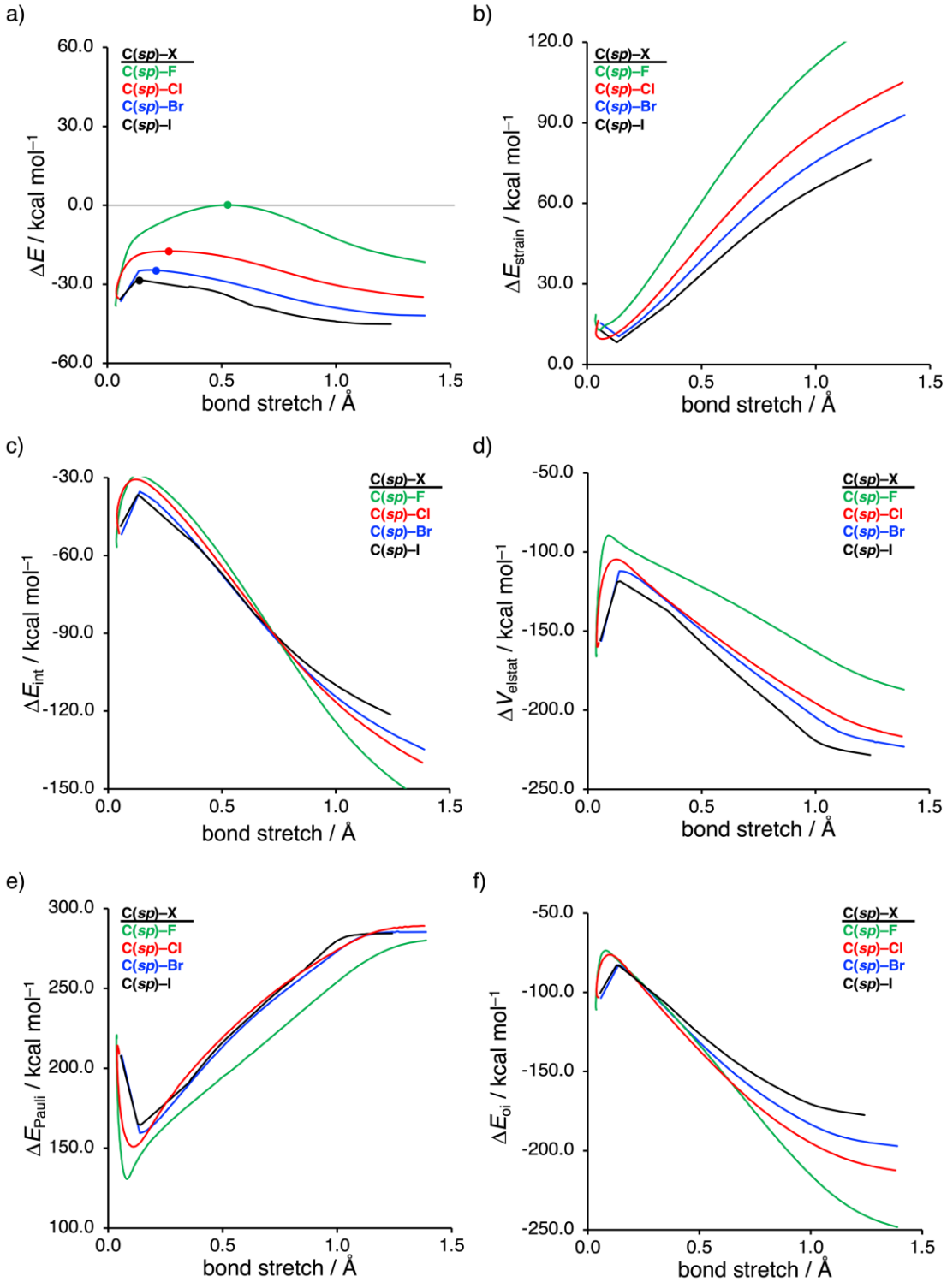

Figure S3.3. Activation strain analyses: a) total energy, b) strain energy, c) interaction energy; and energy decomposition analyses: d) electrostatic interaction, e) Pauli repulsion, and f) orbital interactions, for the oxidative addition of Pd into the C(*sp*)–X bond (X = F, Cl, Br, I), where the transition states are indicated with a dot and the energy terms along the IRC are projected on the C(*sp*)•••X bond stretch. Computed at ZORA-BLYP/TZ2P.

Table S3.2. Decomposition of the Pd–substrate electrostatic interactions (in kcal mol^{-1}) for the oxidative addition of Pd into the C(sp^3)–X bond (X = F, Cl, Br, I).[a,b]

Substrate	Repulsive electrostatic interactions[c]	Attractive electrostatic interactions[d]	Total electrostatic interactions
C(sp^3)–F	309883.3	–309962.6	–79.4
C(sp^3)–Cl	388601.0	–388687.3	–86.3
C(sp^3)–Br	600559.2	–600650.9	–91.7
C(sp^3)–I	795654.4	–795749.1	–94.8

[a] Analyses at consistent geometries obtained from the IRC with a C(sp^3)•••X bond stretch of 0.283 Å at ZORA-BLYP/TZ2P. [b] The interacting reactants are the model bare palladium model catalyst and the substrate C(sp^3)–X. [c] Repulsive electrostatic interactions are the sum of the $\text{nuclear}_{\text{Pd}}$–$\text{nuclear}_{\text{C}(sp3)–\text{X}}$ and $\text{electron}_{\text{Pd}}$–$\text{electron}_{\text{C}(sp3)–\text{X}}$ repulsion. [d] Attractive electrostatic interactions are the sum of the $\text{nuclear}_{\text{Pd}}$–$\text{electron}_{\text{C}(sp3)–\text{X}}$ and $\text{electron}_{\text{Pd}}$–$\text{nuclear}_{\text{C}(sp3)–\text{X}}$ attraction.

Table S3.3. Decomposition of the Pd–substrate electrostatic interactions (in kcal mol^{-1}) for the oxidative addition of Pd into the C(*sp*)–X bond (X = F, Cl, Br, I).[a,b]

Substrate	Repulsive electrostatic interactions[c]	Attractive electrostatic interactions[d]	Total electrostatic interactions
C(*sp*)–F	284466.9	–284570.2	–103.2
C(*sp*)–Cl	370808.7	–370930.4	–121.7
C(*sp*)–Br	559426.1	–559550.6	–124.5
C(*sp*)–I	721061.7	–721189.0	–127.3

[a] Analyses at consistent geometries obtained from the IRC with a C(*sp*)•••X bond stretch of 0.273 Å at ZORA-BLYP/TZ2P. [b] The interacting reactants are the model bare palladium model catalyst and the substrate C(*sp*)–X. [c] Repulsive electrostatic interactions are the sum of the $\text{nuclear}_{\text{Pd}}$–$\text{nuclear}_{\text{C}(sp)–\text{X}}$ and $\text{electron}_{\text{Pd}}$–$\text{electron}_{\text{C}(sp)–\text{X}}$ repulsion. [d] Attractive electrostatic interactions are the sum of the $\text{nuclear}_{\text{Pd}}$–$\text{electron}_{\text{C}(sp)–\text{X}}$ and $\text{electron}_{\text{Pd}}$–$\text{nuclear}_{\text{C}(sp)–\text{X}}$ attraction.

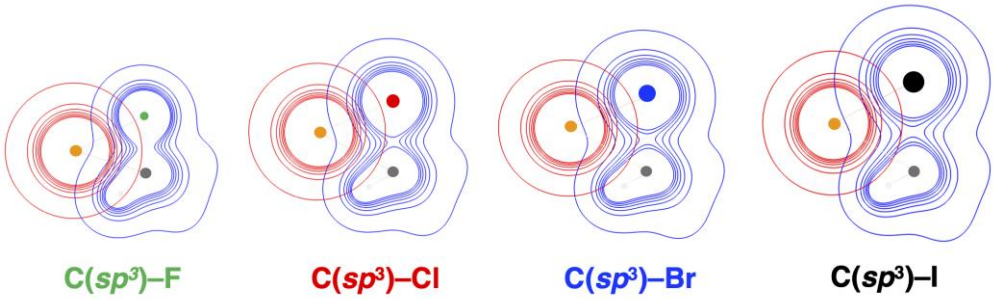

	C(sp^3)–F	C(sp^3)–Cl	C(sp^3)–Br	C(sp^3)–I
r C(sp^3)•••Pd	2.212	2.556	2.637	2.658
r X•••Pd	2.295	2.357	2.449	2.557

Figure S3.4. Density contours from –0.095 to 0.099 Bohr^{-3} for the oxidative addition of Pd into the C(sp^3)–X bond (X = F, Cl, Br, I; electron density of the Pd is shown in red; electron density of C(sp^3)–X substrate in blue; distances in Å) at consistent geometries along the IRC with a C(sp^3)•••X bond stretch of 0.283 Å, computed at ZORA-BLYP/TZ2P. Atoms colors: C = gray, F = green, Cl = red, Br, = blue, I = black, Pd = orange.

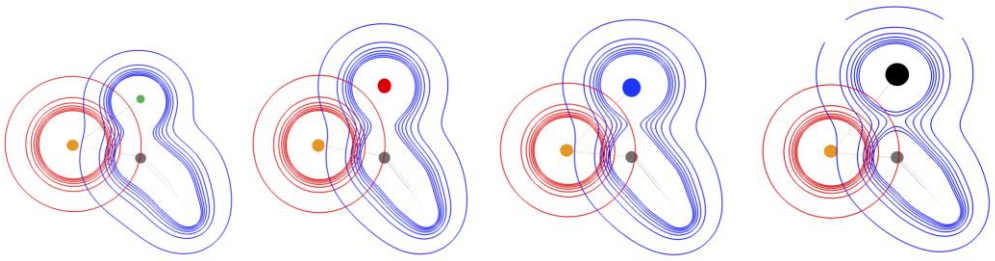

	C(sp)–F	C(sp)–Cl	C(sp)–Br	C(sp)–I
r C(sp)•••Pd	1.934	1.963	1.952	1.943
r X•••Pd	2.252	2.489	2.705	2.843

Figure S3.5. Density contours from –0.095 to 0.099 Bohr^{-3} for the oxidative addition of Pd into the C(sp)–X bond (X = F, Cl, Br, I; electron density of the Pd is shown in red; electron density of C(sp)–X substrate in blue; distances (in Å) at consistent geometries along the IRC with a C(sp)•••X bond stretch of 0.273 Å, computed ZORA-BLYP/TZ2P. Atoms colors: C = gray, F = green, Cl = red, Br, = blue, I = black, Pd = orange.

Declaration by the candidate:

With regard to chapter 4 from pages 57–79, the nature and scope of my contribution were as follows:

Nature of contribution	Extent of contribution (%)
Conceptualization with other authors, Formal analysis, Investigation, Writing – Original Draft, Visualization.	35

The following co-authors have contributed to chapter 4 from pages 57–79:

Name	e-mail address	Nature of contribution	Extent of contribution(%)
Pascal Vermeeren	p.vermeeren@vu.nl	Formal analysis, Writing – Review & Editing, Supervision.	15
Marco Dalla Tiezza	marcodallatiezza@gmail.com	Formal analysis, Writing – Review & Editing, Supervision.	10
Tessel Bouwens	tb764@cam.ac.uk	Formal analysis, Writing – Review & Editing.	10
Catharine Esterhuysen	ce@sun.ac.za	Conceptualization, Formal analysis, Writing – Review & Editing, Supervision, Funding acquisition.	5
Trevor A. Hamlin	t.a.hamlin@vu.nl	Conceptualization, Formal analysis, Writing – Review & Editing, Supervision, Funding acquisition.	10
F. Matthias Bickelhaupt	f.m.bickelhaupt@vu.nl	Conceptualization, Formal analysis,	

		Resources, Writing – Review & Editing, Supervision, Project administration, Funding acquisition.	15

Signature of candidate:……

Date:…23-11-2023……

Declaration by co-authors:

The undersigned hereby confirm that

1. the declaration above accurately reflects the nature and extent of the contributions of the candidate and the co-authors to chapter 4 from pages 57–79,
2. no other authors contributed to chapter 4 from pages 57–79 besides those specified above, and
3. potential conflicts of interest have been revealed to all interested parties and that the necessary arrangements have been made to use the material in chapter 4 from pages 57–79 of this dissertation

Signature	Institutional affiliation	Date
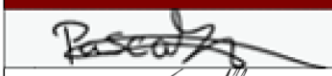	[1]	23-11-2023
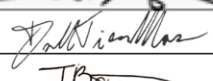	[1]	23 November 2023
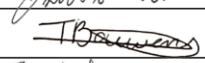	[1]	27 November 2023
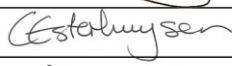	[2]	28 November 2023
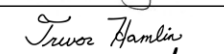	[1]	23 November 2023
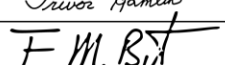	[1], [3], [4]	23 November 2023

[1] Department of Theoretical Chemistry, Amsterdam Institute of Molecular and Life Sciences (AIMMS), and Amsterdam Center for Multiscale Modeling (ACMM), Vrije Universiteit Amsterdam, De Boelelaan 1083, 1081 HV Amsterdam, The Netherlands

[2] Department of Chemistry and Polymer Science, Stellenbosch University, Private Bag X1, Matieland, Stellenbosch, 7602, South Africa

[3] Institute for Molecules and Materials (IMM), Radboud University, Heyendaalseweg 135, 6525 AJ Nijmegen, The Netherlands

[4] Department of Chemical Sciences, University of Johannesburg, Auckland Park, Johannesburg 2006, South Africa.

Chapter 4

Palladium-Catalyzed Activation of $H_nA–AH_n$ Bonds ($AH_n = CH_3, NH_2, OH, F$)

Article Published in Journal of Pure and Applied Chemistry

B.P. Moloto, P. Vermeeren, M. Dalla Tiezza, T. Bouwens,

C. Esterhuysen, T.A. Hamlin, F.M. Bickelhaupt

Pure and Applied Chemistry, ***2023***, *95*, 181–191.

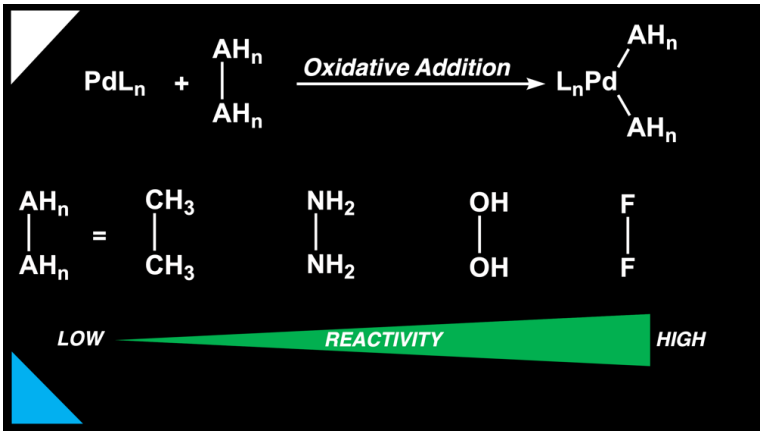

We have quantum chemically studied activation of $H_nA–AH_n$ bonds (AH_n = CH_3, NH_2, OH, F) by PdL_n catalysts with L_n = no ligand, PH_3, $(PH_3)_2$, using relativistic density functional theory at ZORA-BLYP/TZ2P. The activation energy associated with the oxidative addition step decreases from $H_3C–CH_3$ to $H_2N–NH_2$ to HO–OH to F–F, where the activation of the F–F bond is barrierless. Activation strain and Kohn-Sham molecular orbital analyses reveal that the enhanced reactivity along this series of substrates originates from a combination of (i) reduced activation strain due to a weaker $H_nA–AH_n$ bond; (ii) decreased Pauli repulsion as a result of a difference in steric shielding of the $H_nA–AH_n$ bond; and (iii) enhanced backbonding interaction between the occupied 4*d* atomic orbitals of the palladium catalyst and σ* acceptor orbital of the substrate.

4.1. Introduction

Catalysis is intertwined with synthetic chemistry and is of central importance to the chemical industry, as approximately 90% of all industrial processes make use of a catalyst.[1] One of the most prominent catalytic transformations is the palladium-catalyzed cross-coupling reaction, where activated molecular fragments are reacting to form a new bond, typically, between carbon or other main group elements, such as C, N, O, yielding C–C, C–N or C–O bonds, respectively (Scheme 4.1).[2] The catalytic cycle of the palladium-catalyzed cross-coupling begins with the activation of the bond between two cojoined main group elements ($H_nA–AH_n$, AH_n = CH_3, NH_2, OH, F) by oxidative addition to the palladium center. The insertion of Pd into the $H_nA–AH_n$ bond is commonly observed as the rate-determining step[3] and has been subjected to extensive experimental[4] and theoretical studies.[5,6] The next step involves transmetalation where one of the AH_n groups bound to the palladium center is replaced by a hydrocarbon R. In the last step, the original palladium catalyst is regenerated by a reductive elimination step (the reverse of oxidative addition), resulting in a new $H_nA–R$ bond. To enable the design of better performing catalysts in terms of rate and selectivity, a detailed physical understanding of the oxidative addition step is required related to the difference of the electronic and steric properties of the catalyst as well as the $H_nA–AH_n$ bond.

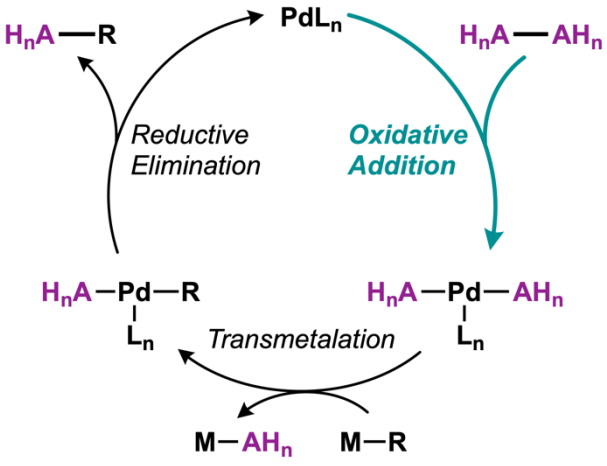

Scheme 4.1. Schematic catalytic cycle of a palladium-catalyzed cross-coupling reaction.

To delineate the effect of varying the nature of the $H_nA–AH_n$ bond on the bond activation process, we have quantum chemically explored the potential energy surface (PES)

of the oxidative insertion of PdL_n, with L_n = no ligand, PH_3, $(PH_3)_2$, into the $H_nA–AH_n$ bond (AH_n = CH_3, NH_2, OH, F), using relativistic density functional theory at ZORA-BLYP/TZ2P (Scheme 2). The activation strain model (ASM)[7] in combination with quantitative Kohn–Sham molecular orbital (KS-MO) theory[8] and a matching energy decomposition analysis (EDA) scheme[9] were employed to unravel the trends in reactivity and provide quantitative insights into the effect of varying AH_n on the $H_nA–AH_n$ bond activation. This computational methodology provides deep physical insight into the factors controlling reactivity and has proven useful for the understanding of, among others, related oxidative addition reactions.[6]

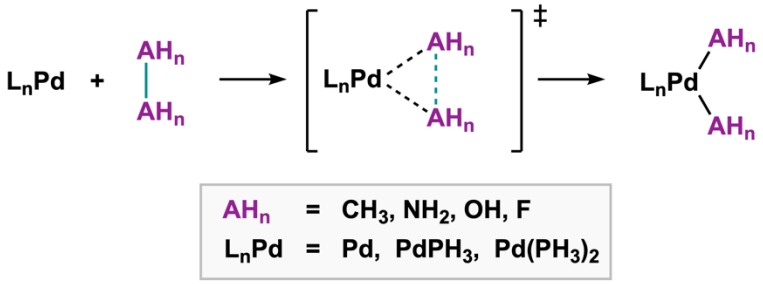

Scheme 4.2. Model oxidative addition reaction between PdL_n and $H_nA–AH_n$, where L_n = no ligand, PH_3, $(PH_3)_2$; and AH_n = CH_3, NH_2, OH, F.

4.2. Computational Methods

Computational Details.

All calculations were executed with the Amsterdam Density Functional (ADF) program.[10] The generalized gradient approximation (GGA) functional BLYP[11] was used for the optimizations of all stationary points and subsequent analyses (spin-unrestricted formalism was used for computing the bond dissociation enthalpies). The basis set used, denoted TZ2P,[12] is of triple-ζ quality and is augmented with two sets of polarization functions on each atom. Scalar relativistic effects were taken into account using the zeroth-order regular approximation (ZORA).[13] This level of theory is denoted as ZORA-BLYP/TZ2P and has been widely tested with several *ab initio* reference benchmarks up until the coupled cluster CCSD(T).[14] The accuracies of the fit scheme (Zlm fit)[15a] and the integration grid (Becke grid)[15b] were set to VERYGOOD. Through vibrational analysis, all stationary points were confirmed to be either

equilibrium structures (zero imaginary frequencies) or transition states (one single imaginary frequency)[16] Furthermore, the normal mode character associated with the imaginary frequency was analyzed to ensure that the correct transition state was found. The potential energy surfaces (PESs) of the studied oxidative addition reactions were obtained by utilizing intrinsic reaction coordinate (IRC) calculations.[17] The acquired PESs were further analyzed using the PyFrag 2019 program[18] Additional calculations including implicit solvation (THF and water) are performed using the conductor-like screening model (COSMO),[19] as implemented in the ADF program. All stationary-point structures were illustrated using CYLview.[20]

Activation Strain Model and Energy Decomposition Analysis

The activation strain model (ASM,[7] also known as the distortion/interaction model[21]) is a fragment-based approach to understand the energy profile of a chemical process in terms of the original reactants, which are the palladium catalyst and the substrate $H_nA–AH_n$. It considers their rigidity and the extent to which the reactants must deform during the reaction plus their ability to interact as the reaction proceeds. In this model, we decompose the total energy, $\Delta E(\zeta)$, into the strain and interaction energy, $\Delta E_{strain}(\zeta)$ and $\Delta E_{int}(\zeta)$, respectively, along the IRC which is projected onto a reaction coordinate ζ that is critically involved in the reaction [Eq. (4.1)].

$$\Delta E(\zeta) = \Delta E_{strain}(\zeta) + \Delta E_{int}(\zeta) \quad (4.1)$$

In this equation, the strain energy, $\Delta E_{strain}(\zeta)$, is the energy required to deform the reactants from their equilibrium structure to the geometry they acquire during the reaction at an arbitrary point ζ of the reaction coordinate. On the other hand, the interaction energy, $\Delta E_{int}(\zeta)$, accounts for all the mutual interactions that occur between the deformed fragments along the reaction coordinate.

The interaction energy between the deformed reactants is further analyzed with the help of our canonical energy decomposition analysis (EDA) scheme.[9] The EDA decomposes the $\Delta E_{int}(\zeta)$ into the following three energy terms [Eq. (4.2)]:

$$\Delta E_{int}(\zeta) = \Delta V_{elstat}(\zeta) + \Delta E_{Pauli}(\zeta) + \Delta E_{oi}(\zeta) \quad (4.2)$$

From this equation, $\Delta V_{elstat}(\zeta)$ is the quasi-classical electrostatic interaction between the unperturbed charge distributions of the deformed reactants. The Pauli repulsion, $\Delta E_{Pauli}(\zeta)$, emerges from the destabilizing interaction between occupied orbitals (more precisely, electrons of same spin) on either of the fragments due to Pauli's exclusion principle. Lastly, the orbital interaction energy, $\Delta E_{oi}(\zeta)$, accounts for charge transfer (*e.g.,* HOMO–LUMO interactions) and polarization between the fragments. A detailed, step-by-step guide on how to perform and interpret the ASM and EDA can be found in Ref. [7c].

In this work, the activation strain and energy decomposition analyses were carried out along the intrinsic reaction coordinate (IRC) projected onto the stretch of the activated $H_nA{\bullet\bullet\bullet}AH_n$ bond, which is a critical geometric parameter of the reaction.[22] This particular geometric parameter undergoes a well-defined change during the reaction going from the reactant complex via the transition state to the product complex and has been shown to be a useful reaction coordinate for studying oxidative addition reactions.[6]

Thermochemistry

The bond dissociation energies (BDE), also known as bond enthalpies (ΔH_{BDE}), are calculated at normal temperature and pressure (NTP, *i.e.*, 298.15 K and 1 atm) from electronic bond energies (ΔE) and vibrational frequencies using the canonical thermochemistry relations for an ideal gas [Eq. (4.3)].[23]

$$\Delta H_{BDE} = \Delta E + \Delta E_{trans,298.15} + \Delta E_{rot,298.15} + \Delta E_{vib,0} + \Delta(\Delta E_{vib,0})_{298.15} \quad (4.3)$$

Herein, $\Delta E_{trans,298.15}$, $\Delta E_{rot,298.15}$, and $\Delta E_{vib,0}$ are the differences in translational, rotational, and zero-point vibrational energy between the $H_nA–AH_n$ substrate and the homolytically dissociated $H_nA^{\bullet}$ radicals. The last term, $\Delta(\Delta E_{vib,0})_{298.15}$, is the vibrational correction energy to bring the system from 0 K to 298.15 K.

4.3. Results and Discussion

We have analyzed the single C–C, N–N, O–O, and F–F bonds in the series $H_nA–AH_n$ (AH_n = CH_3, NH_2, OH, and F). First, we compare the lengths and strengths of these bonds in the different substrates, which are important factors for the overall bond activation (*vide infra*). Table 1 contains the computed bond lengths and bond dissociation enthalpies at ZORA-(U)BLYP/TZ2P. We find that the $H_nA–AH_n$ bond becomes systematically weaker and shorter following the trend from A = C to N to O to F, namely, from 83.2 kcal mol^{-1} and 1.539 Å for $H_3C–CH_3$ to 47.8 kcal mol^{-1} and 1.440 Å for F–F. There is one exception, however, namely, the fact that the bond length does not become shorter from $H_2N–NH_2$ (1.457 Å) to HO–OH (1.495 Å), but longer. This is in line with a previous report where this anomaly in bond length is ascribed to the differing degrees of hyperconjugative stabilization between $H_2N–NH_2$ and HO–OH.[24]

Table 4.1. $H_nA–AH_n$ (AH_n = CH_3, N_2, OH, F) bond lengths (in Å) and bond dissociation enthalpies (ΔH_{BDE}; in kcal mol^{-1}).[a]

Substrate	$H_nA–AH_n$	ΔH_{BDE}
$H_3C–CH_3$	1.539	83.2
$H_2N–NH_2$	1.457	61.4
HO–OH	1.495	52.1
F–F	1.440	47.8

[a] Computed at ZORA-(U)BLYP/TZ2P (enthalpies at 298.15 K and 1 atm).

The results of our ZORA-BLYP/TZ2P exploration are collected in Table 4.2 and Figure 4.1. Full details and additional data can be found in Tables S4.1 and S4.2 and Figures S4.1–S4.3. Note that the overall activation energy $\Delta E^{‡}$, that is, the energy difference between the TS and the infinitely separated reactants (PdL_n and $H_nA–AH_n$), can be negative if a substantially stabilized reactant complex is formed. For a more detailed discussion on the various types of reaction potential energy surfaces, see Reference [25]. The oxidative addition reactions of Pd + $H_nA–AH_n$ (AH_n = CH_3, NH_2, OH, F) generally proceeds via a reactant complex (RC) and a transition state (TS) towards the product complex (PC). Three reactivity trends can be

discerned from the computed reaction profiles. First, the corresponding overall activation energy decreases from +18.7 kcal mol^{-1} for $H_3C–CH_3$ to +7.7 kcal mol^{-1} for $H_2N–NH_2$ to –8.5 kcal mol^{-1} for HO–OH to barrierless for F–F. This latter barrierless process has been previously studied in detail by our group.[26] Second, the coordination of one phosphine ligand to the palladium metal center, *i.e.*, going from Pd to $PdPH_3$, raises the oxidative-addition barrier of the $H_nA–AH_n$ bonds that are more sterically shielded by A–H bonds (i.e., $H_3C–CH_3$ and $H_2N–NH_2$), but it does not affect the reactivity trends along the various bonds compared to the situation for the bare model Pd catalyst. Thus, the highest activation energy is still found for the activation of $H_3C–CH_3$ (+26.4 kcal mol^{-1}), then consistently lowers upon going to HO–OH (–10.1 kcal mol^{-1}) and remains barrierless for the activation of F–F. Third, coordinating two phosphine ligands to the Pd catalyst, *i.e.*, $Pd(PH_3)_2$, further raises the oxidative-addition barrier for the $H_3C–CH_3$ and $H_2N–NH_2$ bonds. Along $H_3C–CH_3$ and $H_2N–NH_2$, the barrier continues to decrease, just as for the model catalysts $PdPH_3$ and Pd. For the activation of the other two substrates, that is, HO–OH and F–F, $Pd(PH_3)_2$ has a major influence on the reaction mode, because (i) it changes the reaction mode of the former towards a stepwise process in which the phosphine ligands play an active role (Figure S4.3); and (ii) the latter substrate reacts via a concerted pathway with an activation energy of –37.0 kcal mol^{-1}.

Table 4.2. Relative energies (kcal mol^{-1}) for the oxidative addition reactions of Pd, $PdPH_3$, and $Pd(PH_3)_2$ with $H_nA–AH_n$ (AH_n = CH_3, NH_2, OH, F) computed in the gas phase.[a,b,c]

Catalyst	Substrate	RC	TS	PC
Pd	$H_3C–CH_3$	–6.7	18.7	–8.7
	$H_2N–NH_2$	–21.4	7.7	–42.8
	HO–OH	–14.6	–8.5	–62.3
	F–F	–44.1	[d]	–100.9
$PdPH_3$	$H_3C–CH_3$	–7.9	26.4	14.1
	$H_2N–NH_2$	–22.4	8.8	–18.7
	HO–OH	–14.5	–10.1	–51.9
	F–F	–42.4	[d]	–101.0
$Pd(PH_3)_2$	$H_3C–CH_3$	0.0	51.8	27.1
	$H_2N–NH_2$	–1.9	38.2	–6.2
	HO–OH	[e]	[e]	[e]
	F–F	–39.8	–37.0	–111.3

[a] Computed at ZORA-BLYP/TZ2P. [b] See Figures 4.1 and S4.1–S4.3 for stationary-point structures. [c] RC = reactant complex ΔE_{RC} TS = activation barrier $\Delta E^{\ddagger}$ PC = product complex ΔE_{rxn} [d] Non-existent: oxidative addition is a barrierless process, see Reference [26]. [e] Follows a different mechanism, see Table S4.2 and Figure S4.3 for full details.

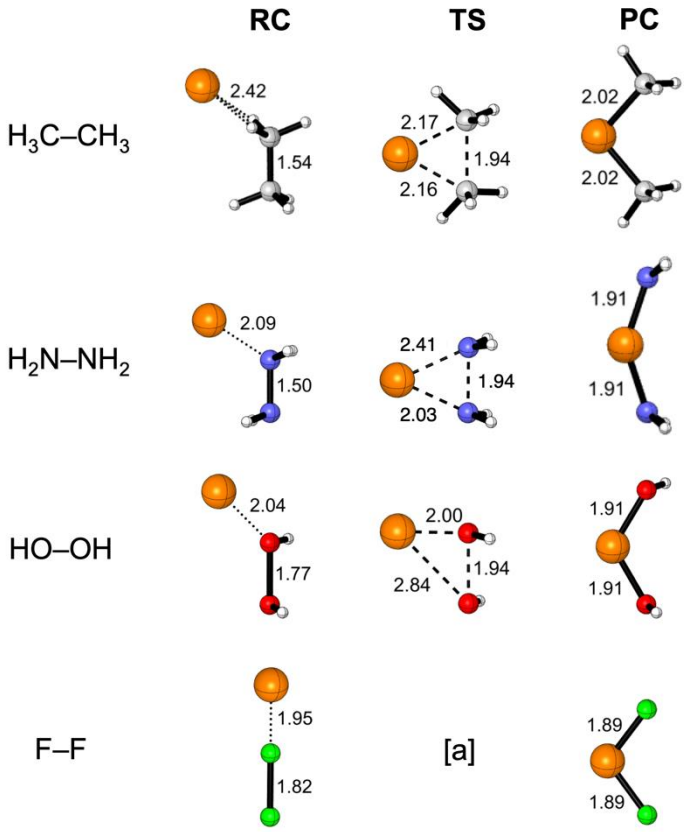

Figure 4.1. Stationary point structures (in Å) for the oxidative addition of Pd + $H_nA–AH_n$ (AH_n = CH_3, NH_2, OH, F) computed in the gas phase at ZORA-BLYP/TZ2P. [a] = Non-existent: oxidative addition into F–F is a barrierless process, see Reference [26]. Atom colors: H = white, C = gray, N = blue, O = red, F = green, Pd = orange.

The computed trends in reactivity are also recovered for bulk solvation computed in THF and water, simulated using COSMO(THF)-ZORA-BLYP/TZ2P and COSMO(water)-ZORA-BLYP/TZ2P. Tables S4.1 and S4.2 report the effect of solvation on the reaction profile of the studied systems. The activation barriers for Pd + $H_nA–AH_n$ (AH_n = CH_3, NH_2, OH, F) are all stabilized by solvation, whereas the activation barriers for both $PdPH_3$ + $H_nA–AH_n$ and $Pd(PH_3)_2$ + $H_nA–AH_n$ are all slightly destabilized. Note that, in solution, the activation of the F–F bond is a barrierless process for all studied catalysts, including $Pd(PH_3)_2$.

To gain quantitative insight into the physical factors governing the oxidative addition reactivity trend, we applied the activation strain model (ASM) of reactivity.[7] Figure 2 displays the activation strain diagrams (ASDs) of the $H_nA–AH_n$ bond activation (AH_n = CH_3, NH_2, OH) by the model bare Pd catalyst along the IRC projected on the $H_nA•••AH_n$ bond stretch. The activation of F–F follows a barrierless process due to the crossing of the singlet and triplet

potential energy surfaces. The underlying physics thereof has previously been studied by our group; we refer the interested reader to Reference [26] for complete details. The bare Pd catalyst is chosen for this detailed analysis, because the simplicity of this model catalyst allows for a lucid picture to emerge from the analyses and because, already for this model catalyst, the universal trend (only $Pd(PH_3)_2$ + HO–OH and F–F constitute exceptions, *vide supra*) of a decreasing activation energy occurs. As shown in Table 4.2, the activation energy goes down from $H_3C–CH_3$ to $H_2N–NH_2$ to HO–OH (Figure 2a), which can be traced back to both the strain and interaction energy (Figure 4.2b and 4.2c). The high activation energy of $H_3C–CH_3$ is the result of the highly destabilizing strain energy for a twofold reason: (i) The $H_3C–CH_3$ is the strongest bond along the investigated series (see Table 4.1): the stronger the bond, *i.e.*, larger ΔH_{BDE}, the harder it is to break, i.e., the more activation strain it generates during the oxidative addition reaction; (ii) the methyl C–H bonds shield the $H_3C–CH_3$ bond, which requires the methyl groups to tilt away from the incoming Pd catalyst.[6]

The lowering of the activation energy upon going from $H_2N–NH_2$ to HO–OH is exclusively the result of the more stabilizing interaction energy, since the strain energies around the transition state for these two substrates are nearly identical. Based on the bond dissociation energies discussed earlier (Table 4.1), one would expect that the stronger $H_2N–NH_2$ bond experiences a more destabilizing strain energy than the HO–OH during the oxidative addition reaction. This is, however, not the case, because the latter experiences additional deformation of the strong O–H bonds, which, in turn, are stronger than N–H bonds,[27] resulting in similar strain energies around the transition states for HO–OH and $H_2N–NH_2$ bond activation.

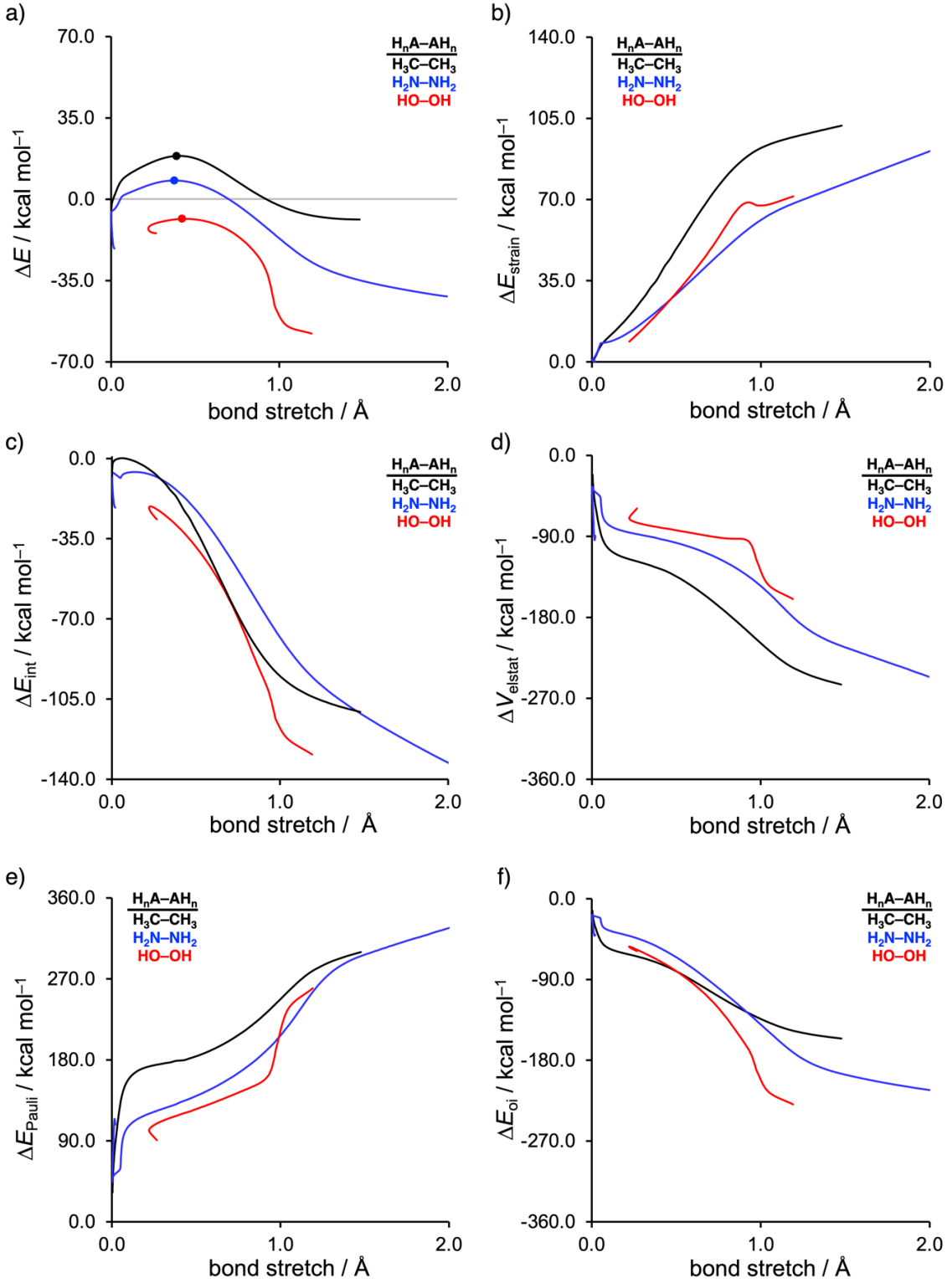

Figure 4.2. Activation strain analyses: (a) total energy, (b) strain energy, (c) interaction energy; and energy decomposition analyses: (d) electrostatic interaction, (e) Pauli repulsion, and (f) orbital interactions, for the oxidative addition reactions of Pd + $H_nA–AH_n$ (AH_n = CH_3, NH_2, OH), where the transition states are indicated with a dot and the energy terms along the IRC are projected on the $H_nA•••AH_n$ bond stretch. Computed at ZORA-BLYP/TZ2P.

Next, we turn to the energy decomposition analysis (EDA)[9] to obtain a better understanding of why the interaction energy becomes more stabilizing when the substrate changes from $H_2N–NH_2$ to HO–OH. The energy decomposition analysis diagrams reveal that the enhanced interaction energy upon going from $H_2N–NH_2$ to HO–OH is a result of two factors, namely, (i) a less destabilizing Pauli repulsion (Figure 4.2e); and (ii) more stabilizing orbital interactions (Figure 4.2f). The electrostatic interactions (Figure 4.2d), on the other hand, are not responsible for the trend in reactivity, because they run counter to the observed reactivity trend.

The origin of the less destabilizing Pauli repulsion for the oxidative addition reaction between Pd and HO–OH compared to $H_2N–NH_2$ was further investigated by performing a Kohn-Sham molecular orbital (KS-MO)[8] analysis (Figure 4.3). The overlap between occupied orbitals of Pd, $H_2N–NH_2$, and HO–OH that engage in a repulsive closed-shell–closed-shell orbital interaction was quantified at consistent geometries obtained from the IRC with a $H_nA•••AH_n$ bond stretch of 0.441 Å. Performing this analysis at a consistent point along the reaction coordinate (near all transition state structures), rather than on the individual transition state structures alone, ensures that the results are not skewed by the position, earlier or later, of the transition state.[7b] For the model bare palladium catalyst, we consider all five occupied 4*d* atomic orbitals ($HOMO_{Pd}$). The participating occupied orbitals of $H_2N–NH_2$ and HO–OH are the π^*-$HOMO_{HnA–AHn}$, where there is a nodal plane between the two AH_n fragments. The closed-shell–closed-shell orbital overlap between the 4*d* AOs of Pd and $H_nA–AH_n$ is the largest for $H_2N–NH_2$ (S = 0.19) and the smallest and, therefore, less destabilizing for HO–OH (S = 0.07) (Figure 4.3a).

The differences in Pauli-orbital overlap originate from the difference in orientation between Pd and $H_nA–AH_n$ (Figure 4.1), which, in turn, is a direct consequence of the degree of steric shielding of the $H_nA–AH_n$ bond by the A–H bonds. The NH_2 groups of $H_2N–NH_2$ have a conformation that shields the direct attack of the Pd catalyst. This differs from the OH groups of HO–OH and hence allows the direct attack of the Pd catalyst for this molecular species. Thus, upon bond activation, the NH_2 groups need to rotate to accommodate the Pd catalyst, thereby forcing the Pd + $H_2N–NH_2$ structure to be symmetric, such that both newly formed

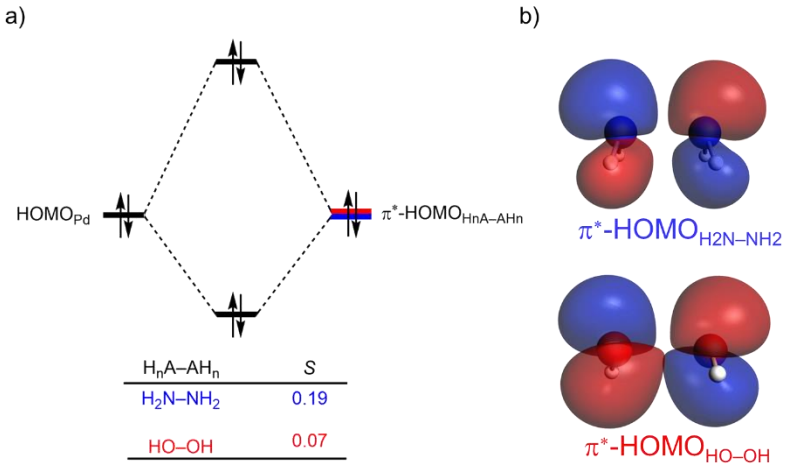

Figure 4.3. a) Schematic molecular orbital diagram of the most important occupied-occupied orbital overlaps, and b) the key occupied molecular orbitals of $H_nA–AH_n$ (isovalue = 0.03 Bohr$^{-3/2}$) of the oxidative addition reaction between Pd and $H_nA–AH_n$ (AH_n = NH_2, OH). Computed at ZORA-BLYP/TZ2P along the IRC projected with a $H_nA•••AH_n$ bond stretch of 0.441 Å.

Pd•••NH_2 bonds are identical in length. Consequently, there are two contact points between the occupied orbitals of Pd and $H_2N–NH_2$, at both NH_2 sides, yielding a large closed-shell–closed-shell orbital overlap and hence Pauli repulsion. For HO–OH, on the other hand, the Pd catalyst can approach the HO–OH bond directly without any need for the OH groups to rotate, due to the absence of steric shielding of the O–H bonds. This gives rise to an asymmetric structure where one newly formed Pd•••OH bond is shorter than the other. As a result, the number of contact points between the occupied orbitals of Pd and HO–OH is reduced, leading to a less destabilizing closed-shell–closed-shell orbital overlap and thus a lower Pauli repulsion.

Finally, we examine why the oxidative addition reaction involving HO–OH proceeds with more stabilizing orbital interactions than $H_2N–NH_2$. Changing the substrate from $H_2N–NH_2$ to HO–OH results in a strengthening of the $HOMO_{Pd}–LUMO_{HnA–AHn}$ backbonding interaction, whereas the $LUMO_{Pd}–HOMO_{HnA–AHn}$ bonding interaction remains nearly constant, as explained in the following (Figure 4.4). By performing a Kohn-Sham molecular orbital (KS-MO) analysis on consistent geometries obtained from the IRC with a $H_nA•••AH_n$ bond stretch of 0.441 Å, we found that the $LUMO_{HnA–AHn}$ drops in energy from –2.4 eV for $H_2N–NH_2$ to –6.0 eV for HO–OH, thereby reducing the $HOMO_{Pd}–LUMO_{HnA–AHn}$ orbital energy gap (Figure 4.4a). The reduction in orbital energy gap, together with the enhanced

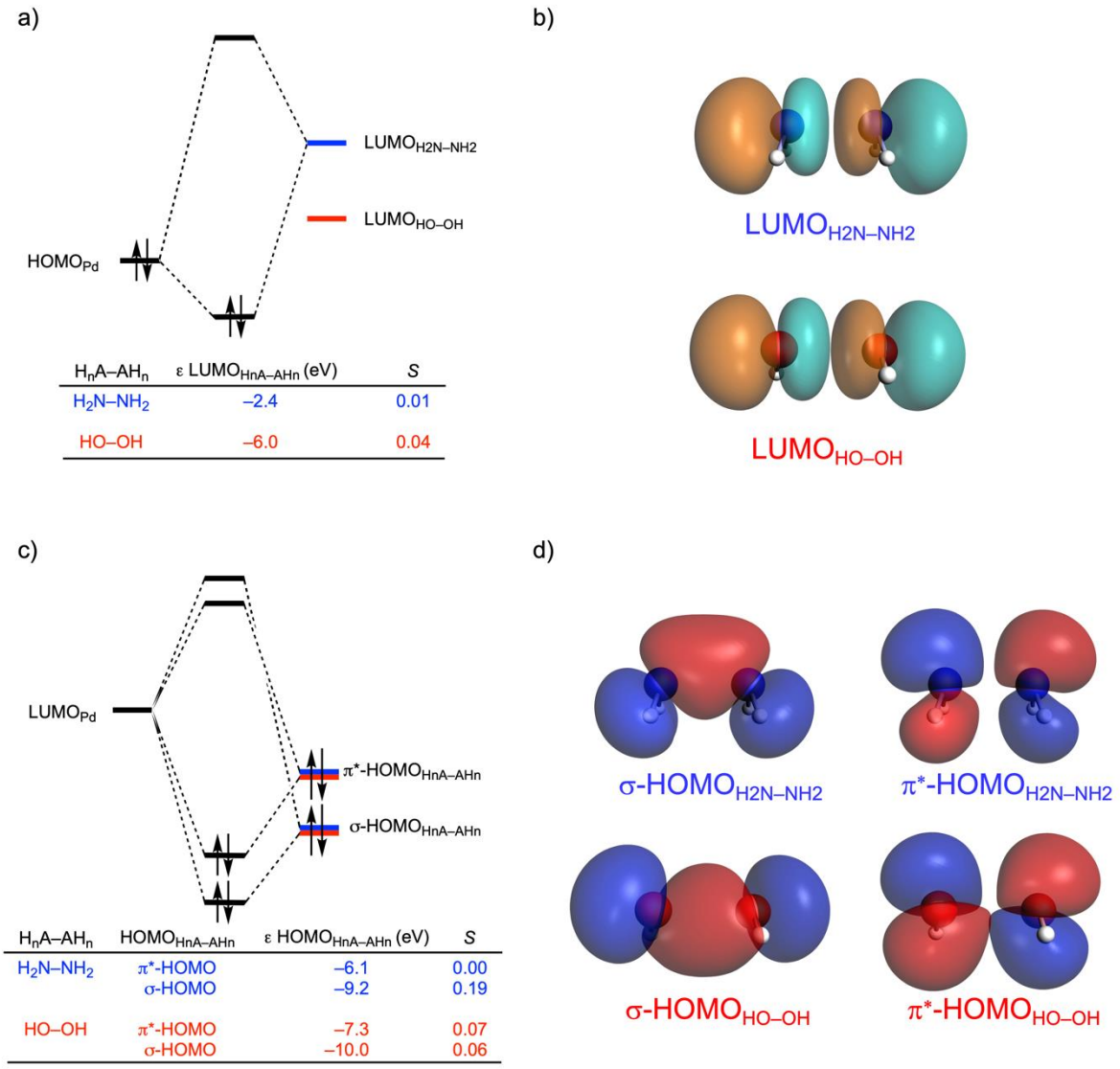

Figure 4.4. Schematic molecular orbital diagram with the key orbital energies and overlaps of a) the HOMO$_{Pd}$–LUMO$_{HnA–AHn}$ backbonding interaction and c) the LUMO$_{Pd}$–HOMO$_{HnA–AHn}$ bonding interaction of the oxidative addition reaction between Pd and H$_n$A–AH$_n$ (AH$_n$ = NH$_2$, OH). The key molecular orbitals of H$_n$A–AH$_n$ contributing to b) the backbonding interaction and d) bonding interaction (isovalue = 0.03 Bohr$^{-3/2}$). Computed at ZORA-BLYP/TZ2P along the IRC projected with a H$_n$A•••AH$_n$ bond stretch of 0.441 Å.

HOMO$_{Pd}$–LUMO$_{HnA–AHn}$ orbital overlap due to the previously discussed difference in orientation between Pd and H$_n$A–AH$_n$, results in a more stabilizing backbonding interaction for HO–OH compared to H$_2$N–NH$_2$. The LUMO$_{Pd}$–HOMO$_{HnA–AHn}$ bonding interaction, on the other hand, remains nearly constant when going from H$_2$N–NH$_2$ to HO–OH, even though the σ-HOMO$_{HO–OH}$ is lower in energy than HOMO$_{H2N–NH2}$, resulting in a larger, less stabilizing, orbital energy gap for the former. HO–OH, however, benefits, due to the approach of the

reactants, from an additional stabilizing bonding interaction between $LUMO_{Pd}$–π^*-$HOMO_{HO–OH}$, thereby recovering the bonding orbital interactions (Figure 4.4c).

4.4 Conclusions

The activation barrier for palladium-mediated $H_nA–AH_n$ bond activation decreases systematically along the series $H_3C–CH_3$ to $H_2N–NH_2$ to HO–OH to F–F. The activation of the F–F bond is even barrierless. This follows from our quantum chemical exploration of the A–A oxidative addition to palladium in the model reactions of $PdL_n + H_nA–AH_n$ (L_n = no ligand, PH_3, $(PH_3)_2$; AH_n = CH_3, NH_2, OH, F), using relativistic density functional theory.

Our detailed activation strain and Kohn-Sham molecular orbital analyses reveal that the decreased oxidative addition reaction barrier upon going from $H_3C–CH_3$ to $H_2N–NH_2$ to HO–OH to F–F mainly originates from the difference in bond strength along this series which decreases along this series. The $H_3C–CH_3$ bond is the strongest bond along the investigated series. The stronger the bond, the more energy it costs to break, and hence the more activation strain it generates during the oxidative addition reaction. Furthermore, the methyl C–H bonds shield the $H_3C–CH_3$ bond, which requires the methyl groups to bend away from the incoming Pd catalyst, generating additional activation strain.

The activation barrier lowers further from $H_2N–NH_2$ to HO–OH due to two additional barrier lowering phenomena, namely, (i) a less destabilizing steric (Pauli) repulsion; and (ii) more stabilizing orbital interactions. The former effect is a result of the difference in steric shielding of the $H_nA–AH_n$ bond by the AH_n groups. The NH_2 groups of $H_2N–NH_2$ have a conformation that shields the N–N bond, forcing the Pd catalyst to attack the bond more side-on and hence yields a large closed-shell–closed-shell orbital overlap and Pauli repulsion. In the case of HO–OH, the absence of steric shielding of the OH groups allows the direct attack of the Pd catalyst, resulting in less contact points between the occupied orbitals of the reactants and hence decreased Pauli repulsion. The more stabilizing orbital interactions, on the other hand, originate from the energetically lower-lying σ* acceptor orbital of HO–OH compared to $H_2N–NH_2$ that can engage in a strong backbonding interaction with the occupied 4*d* atomic orbitals of the palladium catalyst. Finally, the activation of the F–F bond is a barrierless process due to the crossing of the singlet and triplet potential energy surfaces, as has been described in detail by de Jong *et al*.[26]

4.5 References

[1] a) J. Collman, L. Hegedus, J. Norton, R. Finke, *Principles and Applications of Organotransition Metal Chemistry*, **1987**; b) F. Diederich, P. J. Stang, *Metal-Catalyzed Cross-Coupling Reactions*, Wiley-VCH, Weinheim, **1998**; c) J. F. Hartwig, *Organotransition Metal Chemistry: From Bonding to Catalysis*, University Science Books, Sausalito, **2010**; d) P. W. N. M. van Leeuwen, *Homogeneous Catalysis: Understanding the Art*, Kluwer Academic Publishers, Dordrecht, **2004**; e) L. Souillart, N. Cramer, *Chem. Rev.* **2015**, *115*, 9410.

[2] a) C. C. C. Johansson Seechurn, M. O. Kitching, T. J. Colacot, V. Snieckus, *Angew. Chem. Int. Ed.* **2012**, *51*, 5062; b) E.-I. Negishi, *Angew. Chem. Int. Ed.* **2011**, *50*, 6738; c) A. Suzuki, *Angew. Chem. Int. Ed.* **2011**, *50*, 6722.

[3] a) G. B. Smith, G. C. Dezeny, D. L. Hughes, A. O. King, T. R. Verhoeven, *J. Org. Chem.* **1994**, *59*, 8151; b) Hydrogenation. In Homogeneous Catalysis, Springer Netherlands, Dordrecht, **2004**, pp. 75–100. c) B. Crociani, S. Antonaroli, L. Canovese, P. Uguagliati, F. Visentin, *Eur. J. Inorg. Chem.* **2004**, 732; d) R. van Asselt, K. Vrieze, C. J. Elsevier, *J. Org. Chem.* **1994**, *480*, 27.

[4] a) J. C. Weisshaar, *Acc. Chem. Res.* **1993**, *26*, 213; b) A. E. Shilov, G. B. Shul'pin, *Chem. Rev.* **1997**, *97*, 2879; c) M. E. van der Boom, D. Milstein, *Chem. Rev.* **2003**, *103*, 1759; d) R. H. Crabtree, *J. Organomet. Chem.* **2004**, *689*, 4083; e) C.-H. Jun, *Chem. Soc. Rev.* **2004**, *33*, 610; f) M. Lersch, M. Tilset, *Chem. Rev.* **2005**, *105*, 2471; g) J. R. Hummel, J. A. Boerth, J. A. Ellman, *Chem. Rev.* **2016**, *117*, 9163.

[5] a) S. Niu, M. B. Hall, *Chem. Rev.* **2000**, *100*, 353; b) M. Torrent, M. Solà, G. Frenking, *Chem. Rev.* **2000**, *100*, 439; c) A. Dedieu, *Chem. Rev.* **2000**, *100*, 543; d) S. Kozuch, C. Amatore, A. Jutand, S. Shaik, *Organometallics* **2005**, *24*, 2319; e) L. Xue, Z. Lin, *Chem. Soc. Rev.* **2010**, *39*, 1692; f) D. Balcells, E. Clot, O. Eisenstein, *Chem. Rev.* **2010**, *110*, 749; g) M. Besora, C. Gourlaouen, B. Yates, F. Maseras, *Dalton Trans.* **2011**, *40*, 11089; h) M. Garcia-Melchor, A. A. Braga, A. Lledos, G. Ujaque, F. Maseras, *Acc. Chem. Res.* **2013**, *46*, 2626; i) J. Joy, T. Stuyver, S. Shaik, *J. Am. Chem. Soc.* **2020**, *142*, 3836; j) M. C. D'Alterio, E. Casals-Cruañas, N. V. Tzouras, G. Talarico, S. P. Nolan, A. Poater, *Chem. Eur. J.* **2021**, *27*,12481.

[6] a) P. Vermeeren, X. Sun, F. M. Bickelhaupt, *Sci. Rep.* **2018**, *8*, 10729; b) L. P. Wolters, W.-J. van Zeist, F. M. Bickelhaupt, *Chem. Eur. J.* **2014**, *20*, 11370; c) L. P. Wolters, F. M. Bickelhaupt, *Chem. Asian J.* **2015**, *10*, 2272; d) T. Hansen, X. Sun, M. Dalla Tiezza, W. -J. van Zeist, J. N. P. van Stralen, D. P. Geerke, L. P. Wolters, T. A. Hamlin, F. M. Bickelhaupt, *Chem. Eur. J.* **2022**, e202201093; e) T. Hansen, X. Sun, M. Dalla Tiezza, W. -J. van Zeist, J. Poater, T. A. Hamlin, F. M. Bickelhaupt, *Chem. Eur. J.* **2021**, e202103963; f) B. P. Moloto, P. Vermeeren, M. Dalla Tiezza, C. Esterhuysen, F. M. Bickelhaupt, T. A. Hamlin, *Eur. J. Org. Chem.* **2022**, DOI: 10.1002/ejoc.202200722.

[7] For reviews, see: a) F. M. Bickelhaupt, K. N. Houk, *Angew. Chem.* **2017**, *129*, 10204; *Angew. Chem. Int. Ed.* **2017**, *56*, 10070; b) P. Vermeeren, T. A. Hamlin, F. M.

Bickelhaupt, *Chem Commun.* **2021**, *57*, 5880; For a step-by-step protocol, see: c) P. Vermeeren, S. C. C. van der Lubbe, C. Fonseca Guerra, F. M. Bickelhaupt, T. A. Hamlin, *Nat. Protoc.* **2020**, *15*, 649.

[8] a) R. van Meer, O. V. Gritsenko, E. J. Baerends, *J. Chem. Theory Comput.* **2014**, *10*, 4432; b) T. A. Albright, J. K. Burdett, M.-H. Whangbo, *Orbital Interactions in Chemistry*, John Wiley & Sons, Inc., **2013**.

[9] For an overview of the EDA method, see: a) T. A. Hamlin, P. Vermeeren, C. Fonseca Guerra, F. M. Bickelhaupt, in *Complementary Bonding Analysis*, (Ed. S. Grabowsky), De Gruyter, Berlin, **2021**, pp. 199–212; for a detailed overview of the EDA method, see: b) F. M. Bickelhaupt, E. J. Baerends, in *Reviews in Computational Chemistry*, (Eds. K. B. Lipkowitz, D. B. Boyd), Wiley, Hoboken, **2000**, pp. 1–86.

[10] a) G. te Velde, F. M. Bickelhaupt, E. J. Baerends, C. Fonseca Guerra, S. J. A. van Gisbergen, J. G. Snijders, T. Ziegler, *J. Comput. Chem.* **2001**, *22*, 931; b) C. Fonseca Guerra, J. G. Snijders, G. te Velde, E. J. Baerends, *Theor. Chem. Acc.* **1998**, *99*, 391; c) ADF2019.102, SCM Theoretical Chemistry, Vrije Universiteit: Amsterdam (Netherlands). http://www.scm.com.

[11] a) A. D. Becke, *Phys. Rev. A* **1988**, *38*, 3098; b) B. G. Johnson, P. M. W. Gill, J. A. Pople, *J. Chem. Phys.* **1993**, *98*, 5612; c) C. Lee, W. Yang, R. G. Parr, *Phys. Rev. B* **1988**, *37*, 785; d) T. V. Russo, R. L. Martin, P. J. Hay, *J. Chem. Phys.* **1994**, *101*, 7729.

[12] E. van Lenthe, E. J. Baerends, *J. Chem. Phys.* **2003**, *24*, 1142.

[13] a) E. van Lenthe, E. J. Baerends, J. G. Snijders, *J. Chem. Phys.* **1993**, *99*, 4597; b) E. van Lenthe, E. J. Baerends, J. G. Snijders, *J. Chem. Phys.* **1994**, *101*, 9783; c) E. van Lenthe, A. Ehlers, E. J. Baerends, *J. Chem. Phys.* **1999**, *110*, 8943.

[14] a) G. T. de Jong, M. Solà, L. Visscher, F. M. Bickelhaupt, *J. Chem. Phys.* **2004**, *121*, 9982; b) G. T. de Jong, D. P. Geerke, A. Diefenbach, F. M. Bickelhaupt, *J. Chem. Phys.* **2005**, *313*, 261; c) G. T. De Jong, D. P. Geerke, A. Diefenbach, M. Solà, F. M. Bickelhaupt, *J. Comput. Chem.* **2005**, *26*, 1006; d) G. Th. de Jong, F. M. Bickelhaupt, *J. Phys. Chem. A*, **2005**, *109*, 9685.

[15] a) M. Franchini, P. H. T. Philipsen, E. van Lenthe, L. Visscher, *J. Chem. Theory Comput.* **2014**, *10*, 1994; b) M. Franchini, P. H. T. Philipsen, L. Visscher, *J. Comput. Chem.* **2013**, *34*, 1819.

[16] a) A. Bérces, R. M. Dickson, L. Fan, H. Jacobsen, D. P. Swerhone, T. Ziegler, *Comput. Phys. Commun.* **1997**, *100*, 247; b) H. Jacobsen, A. Bérces, D. P. Swerhone, T. Ziegler, *Comput. Phys. Commun.* **1997**, *100*, 263; c) S. K. Wolff, *Int. J. Quantum Chem.* **2005**, *104***,** 645.

[17] a) K. Fukui, *Acc. Chem. Res.* **1981**, *14*, 363; b) L. Deng, T. Ziegler, L. Fan, *J. Chem. Phys.* **1993**, *99*, 3823; c) L. Deng, T. Ziegler, *Int. J. Quantum Chem.* **1994**, *52*, 731.

[18] a) X. Sun, T. M. Soini, J. Poater, T. A. Hamlin, F. M. Bickelhaupt, *J. Comput. Chem.* **2019**, *40*, 2227; b) PyFrag 2019: X. Sun, T. Soini, L. P. Wolters, W.-J. van Zeist, C.

Fonseca Guerra, T. A. Hamlin, F. M. Bickelhaupt, Vrije Universiteit Amsterdam, The Netherlands.

[19] a) A. Klamt, G. Schüürmann, *J. Chem. Soc. Perkin Trans. 2* **1993**, 799; b) A. Klamt, *J. Phys. Chem.* **1995**, 2224; c) A. Klamt, V. Jonas, *J. Chem. Phys.* **1996**, *105*, 9972; d) C. C. Pye, T. Ziegler, *Theor. Chem. Acc.* **1999**, *101*, 396.

[20] CYLview2.0; C. Y. Legault, Université de Sherbrooke, 2020 (http://www.cylview.org).

[21] a) D. H. Ess, K. Houk, *J. Am. Chem. Soc.* **2007**, *129*, 10646; b) D. H. Ess, K. Houk, *J. Am. Chem. Soc.* **2008**, *130*, 10187.

[22] W.-J. van Zeist, A. H. Koers, L. P. Wolters, F. M. Bickelhaupt, *J. Chem. Theory Comput.* **2008**, *4*, 920.

[23] a) D. A. McQuarrie, J. D. Simon, Physical Chemistry: A Molecular Approach, University Science Books, Sausalito, Calif, **1997**; b) C. J. Cramer, Essentials of Computational Chemistry: Theories and Models, Wiley, Chichester, West Sussex, England; Hoboken, NJ, **2004**; c) F. Jensen, Introduction to Computational Chemistry, Wiley, Chichester, UK; Hoboken, NJ, **2017**; d) P. W. Atkins, J. De Paula, J. Keeler, Atkins' Physical Chemistry, Oxford University Press, Oxford, United Kingdom; New York, NY, **2018**.

[24] a) D. J. Mckay, J. S. Wright, *J. Am. Chem. Soc.* **1998**, *120*, 1003; b) L. Song, M. Liu, W. Wu, Q. Zhang, Y. Mo, *J. Chem. Theory Comput.* **2005**, *1*, 394.

[25] F. M. Bickelhaupt, *Mass Spectrom. Rev.* **2001**, *20*, 347.

[26] For a detailed discussion of Pd + F–F reaction, see: G. T. de Jong, A. Kovács, F. M. Bickelhaupt, *J. Phys. Chem. A.* **2006**, *110*, 7943.

[27] a) B. Ruscic, J. Berkowitz, *J. Chem. Phys.* **1991**, *95*, 4378; b) S. W. Benson, *J. Chem. Educ.* **1965**, *42*, 502.

4.6 Supporting Information

Table S4.1. Computed relative energies (kcal mol^{-1}) for the oxidative addition reactions of Pd, $PdPH_3$, and $Pd(PH_3)_2$ with $H_nA–AH_n$ (AH_n = CH_3, NH_2, OH, F) in THF and aqueous solution.[a]

Catalyst	Substrate	RC		TS		PC	
		THF	Water	THF	Water	THF	Water
Pd	$H_3C–CH_3$	–7.5	–7.6	17.5	17.3	–10.6	–10.9
	$H_2N–NH_2$	–22.5	–22.8	5.5	6.8	–40.6	–40.0
	HO–OH	–18.6	–21.0	–16.2	–19.3	–64.7	–65.3
	F–F	–67.0	–76.0	[b]	[b]	–113.4	–116.0
$PdPH_3$	$H_3C–CH_3$	–7.0	–6.9	27.5	27.7	13.9	13.6
	$H_2N–NH_2$	–21.2	–21.1	12.4	12.9	–17.5	–17.7
	HO–OH	–12.0	–11.8	–8.8	–9.3	–55.6	–57.1
	F–F	–72.5	–86.8	[b]	[b]	–116.6	–121.3
$Pd(PH_3)_2$	$H_3C–CH_3$	0.0	[c]	53.7	54.2	25.9	25.5
	$H_2N–NH_2$	–0.9	–0.7	41.9	43.7	–8.5	–10.3
	HO–OH	[c]	[c]	[c]	[c]	[c]	[c]
	F–F	[b]	[b]	[b]	[b]	–131.2	–137.7

[a] Computed at COSMO(THF)-ZORA-BLYP/TZ2P and COSMO(water)-ZORA-BLYP/TZ2P. [b] Non-existent: oxidative addition is a barrierless process. [c] Follows a different mechanism.

Table S4.2. Computed relative energies (kcal mol^{-1}) for the oxidative addition reactions of $Pd(PH_3)_2$ + HO–OH in the gas-phase, and in THF and aqueous solution.

Systems		$Pd(PH_3)_2$		
		Gas Phase[a]	THF[b]	Water[c]
HO–OH	TS1	1.3	[d]	[d]
	INT1	1.1	[d]	[d]
	TS2	2.5	[d]	[d]
	INT2	–63.0	–67.9	–69.4
	TS3	–28.3	–33.5	–35.8
	PC	–51.3	–58.2	–63.3

[a] Computed at ZORA-BLYP/TZ2P. [b] Computed at COSMO(THF)-ZORA-BLYP/TZ2P. [c] Computed at COSMO(water)-ZORA-BLYP/TZ2P. [d] Non-existent.

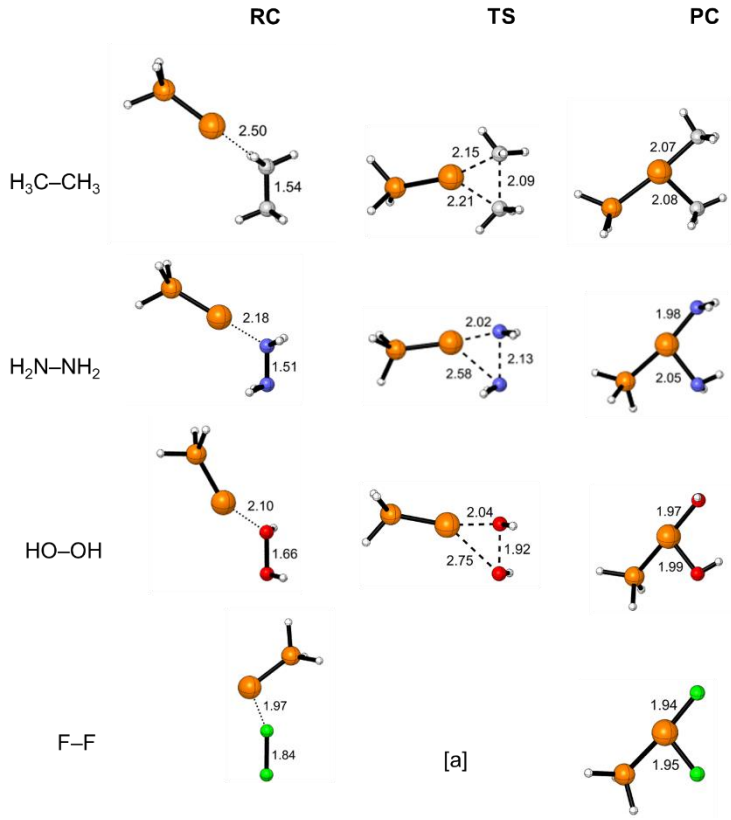

Figure S4.1. Stationary point structures (in Å) for the oxidative addition of $PdPH_3$ + $H_nA–AH_n$ (AH_n = CH_3, NH_2, OH, F) in the gas phase, computed at ZORA-BLYP/TZ2P. Atom colors: H = white, C = gray, N = blue, O = red, F = green, P = orange (small), Pd = orange (large).

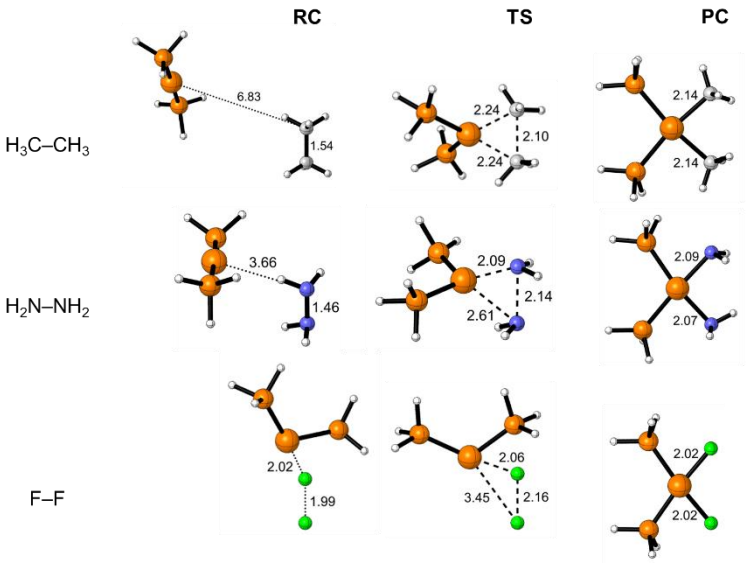

Figure S4.2. Stationary point structures (in Å) for the oxidative addition of $Pd(PH_3)_2$ + H_nA–AH_n (AH_n = CH_3, NH_2, F) in the gas phase, computed at ZORA-BLYP/TZ2P. Atom colors: H = white, C = gray, N = blue, P = orange (small), Pd = orange (large).

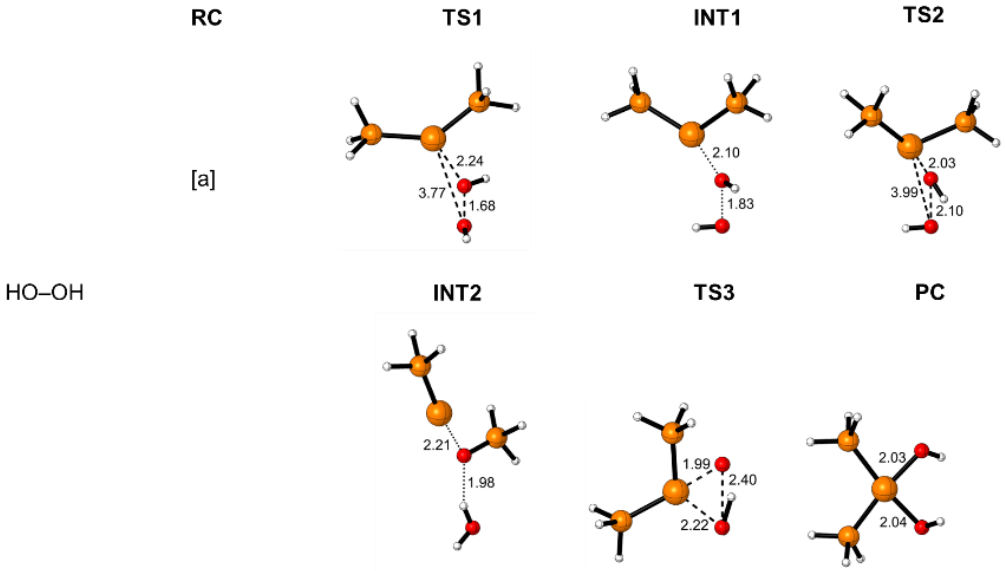

Figure S4.3. Stationary point structures (in Å) for the oxidative addition of a) $Pd(PH_3)_2$ + HO–OH in the gas phase, computed at ZORA-BLYP/TZ2P. [a] = Non-existent RC. Atom colors: H = white, O = red, F = green, P = orange (small), Pd = orange (large).

Summary

This thesis focuses on investigating fundamental oxidative addition (OA) reactions catalysed by palladium (see Chapter 1). OA, being the first and rate determining step in cross-coupling reactions, is a reaction of vital importance in synthetic chemistry. Palladium-catalysed cross-coupling reactions are widely used in industrial applications, such as in catalytic converters and the synthesis of pharmaceuticals. Besides these applications, palladium is widely used as a versatile catalytic reagent in many different chemical processes. Considering the importance of oxidative addition reactions catalysed by palladium, a deep understanding of the underlying mechanism is crucial to designing new catalysts and improving the existing ones. In a nutshell, the main focus is on understanding the mechanism behind the oxidative addition step and the trends in activation barriers upon variation of either the catalyst or substrate structure. The following summary will discuss only the most important findings from the chapters involved.

As explained in Chapter 2, the findings in this thesis were successfully obtained using the Activation Strain Model of chemical reactivity (ASM, discussed in section 2.3) in combination with computations based on Density Functional Theory (DFT) as implemented in the ADF program. The ASM model is a fragment-based approach that characterizes reactions in terms of the rigidity and the bonding capabilities of the original reactants , and the extent to which the reactants must deform along the reaction pathway of a particular reaction mechanism. Thus, the total energy profile of a particular chemical reaction can be decomposed into contributions from the deformation of the reactants (the strain energy) and their mutual interaction (the interaction energy). The interaction energy can then be further decomposed using the canonical energy decomposition analysis (EDA) of ADF into electrostatic interactions, destabilizing Pauli repulsion, and stabilizing orbital interactions.

In Chapter 3, with the aim of understanding the underlying mechanism and trends found by the oxidative addition, we detailed our quantum chemical exploration of the palladium-mediated activation of C(sp^n)–X bonds (n = 1–3; X = F, Cl, Br, I) in the archetypal model substrates $H_3C–CH_2–X$, $H_2C=CH–X$, and HC≡C–X by a model bare palladium catalyst. First and foremost, we investigated the bond dissociation enthalpies (BDEs) of the bonds to be activated. So, we started from the C(sp^3)–X moving to C(sp^2)–X and then to C(sp)–X bonds for each of the selected set of X atoms above. We found that as we move down group 17, the

C(sp^n)–X bond becomes weaker and as such easier to break. Based on our state-of-the-art analyses, we discovered that as we vary the substituent X, going down Group 17 from X = F to Cl to Br to I on the C(sp^n)–X substrate, the oxidative addition barriers drastically decrease. This favorable activation barrier stabilization originates from two factors: (i) a less destabilizing activation strain; and remarkably (ii) a more favorable electrostatic attraction between the catalyst and the substrate. When changing the substrate from C(sp^n)–F to C(sp^n)–I, consequently, the electrostatic interaction between the catalyst and substrate also becomes more favorable. Iodine, being the largest halogen of the selected substituents, has a more diffuse and electron-rich density and a higher nuclear charge that in turn engage in favorable electrostatic attractions with the palladium nucleus and electron density, respectively. This effect makes the oxidative addition reaction involving the C(sp^n)–X bond with a larger halogen atom correspond to a more stabilizing interaction and hence lower reaction barrier.

Next, in Chapter 4 we have quantum chemically investigated the palladium-mediated activation of $H_nA–AH_n$ bonds (AH_n = CH_3, NH_2, OH, F) by catalysts PdL_n with L_n = no ligand, PH_3, $(PH_3)_2$. Herein, we found that as we move from C to F along the period, i.e., from $H_3C–CH_3$ to $H_2N–NH_2$ to HO–OH to F–F, the activation barriers decrease and more interestingly the activation of the F–F bond is even barrierless. As we move from C to F on the selected substrates, the number of the substituents around the A–A bond become less and as such enabling the catalyst to approach the substrate with ease, thereby resulting in a decreasing activation barriers. The causal effects of this barrier stabilizations stem from: (i) a reduced activation strain due to a weaker $H_nA–AH_n$ bond; (ii) a decreased Pauli repulsion as a result of a difference in steric shielding of the $H_nA–AH_n$ bond; and (iii) an enhanced backbonding interaction between the occupied 4*d* atomic orbitals of the palladium catalyst and σ* acceptor orbital of the substrate.

The findings in this thesis have the potential to equip experimentalists with detailed mechanistic insight that can facilitate a deep understanding into the trends in reactivity of palladium-mediated oxidative addition reactions.

Samenvatting

Dit proefschrift richt zich op het onderzoeken van fundamentele oxidatieve additie (OA) reacties gekatalyseerd door palladium (zie Hoofdstuk 1). OA, de eerste en snelheidsbepalende stap in kruiskoppelingsreacties, is een reactie van vitaal belang in de synthetische chemie. Door palladium gekatalyseerde kruiskoppelingsreacties worden veel gebruikt in industriële toepassingen, zoals in katalysatoren en de synthese van geneesmiddelen. Naast deze toepassingen wordt palladium veel gebruikt als een veelzijdig katalytisch reagens in veel verschillende chemische processen. Gezien het belang van oxidatieve additiereacties gekatalyseerd door palladium, is een goed begrip van het onderliggende mechanisme cruciaal voor het ontwerpen van nieuwe katalysatoren en het verbeteren van de bestaande. In een notendop, de belangrijkste focus ligt op het begrijpen van het mechanisme achter de oxidatieve additiestap en de trends in activeringsbarrières bij variatie van de katalysator- of substraatstructuur. In de volgende samenvatting worden alleen de belangrijkste bevindingen uit de betrokken hoofdstukken besproken.

Zoals uitgelegd in Hoofdstuk 2, zijn de bevindingen in dit proefschrift met succes verkregen met behulp van het Activation Strain Model van chemische reactiviteit (ASM, besproken in paragraaf 2.3) in combinatie met berekeningen gebaseerd op Dichtheidsfunctionaal-theorie (DFT) zoals geïmplementeerd in het ADF programma. Het ASM model is een op fragmenten gebaseerde benadering die reacties karakteriseert in termen van de stijfheid en het hechtingsvermogen van de oorspronkelijke reactanten, en de mate waarin de reactanten langs het reactiepad van een bepaald reactiemechanisme moeten vervormen. Het totale energieprofiel van een bepaalde chemische reactie kan dus worden ontleed in bijdragen van de vervorming van de reactanten (de spanningsenergie) en hun onderlinge interactie (de interactie-energie). De interactie-energie kan vervolgens verder worden ontleed met behulp van de canonieke energie-ontledingsanalyse (EDA) van ADF in elektrostatische interacties, destabiliserende Pauli-afstoting en stabiliserende orbitaalinteracties.

In Hoofdstuk 3, met als doel het onderliggende mechanisme en de trends gevonden door de oxidatieve additie te begrijpen, hebben we onze kwantumchemische verkenning van de palladium-gemedieerde activering van C(sp^n)–X bindingen (n = 1–3; X = F, Cl, Br, I) in de archetypische modelsubstraten $H_3C–CH_2–X$, $H_2C=CH–X$ en HC≡C–X door een model-kale

palladiumkatalysator. Eerst en vooral onderzochten we de bindingsdissociatie-enthalpieën (BDE's) van de te activeren bindingen. We zijn dus begonnen met de C(sp^3)–X naar C(sp^2)–X en vervolgens naar C(sp)–X bindingen voor elk van de geselecteerde set X-atomen hierboven. We ontdekten dat naarmate we naar beneden gaan in groep 17, de C(sp^n)–X binding zwakker wordt en als zodanig gemakkelijker te verbreken is. Op basis van onze state-of-the-art analyses ontdekten we dat als we de substituent X variëren, van groep 17 van X = F naar Cl naar Br naar I op het C(sp^n)–X substraat, de oxidatieve additiebarrières drastisch verminderen. Deze gunstige stabilisatie van de activeringsbarrière is het gevolg van twee factoren: (i) een minder destabiliserende activeringsstam; en opmerkelijk genoeg (ii) een gunstiger elektrostatische aantrekking tussen de katalysator en het substraat. Bij het veranderen van het substraat van C(sp^n)–F naar C(sp^n)–I wordt bijgevolg ook de elektrostatische interactie tussen de katalysator en het substraat gunstiger. Jodium, dat het grootste halogeen is van de geselecteerde substituenten, heeft een meer diffuse en elektronenrijke dichtheid en een hogere nucleaire lading die op hun beurt gunstige elektrostatische aantrekkingskracht uitoefenen met respectievelijk de palladiumkern en elektronendichtheid. Dit effect zorgt ervoor dat de oxidatieve additiereactie waarbij de C(sp^n)–X binding met een groter halogeenatoom betrokken is, overeenkomt met een meer stabiliserende interactie en dus een lagere reactiebarrière.

Vervolgens hebben we in Hoofdstuk 4 kwantumchemisch onderzoek gedaan naar de palladium-gemedieerde activering van $H_nA–AH_n$ bindingen (AH_n = CH_3, NH_2, OH, F) door katalysatoren PdL_n met L_n = geen ligand, PH_3, $(PH_3)_2$. Hierin ontdekten we dat naarmate we van C naar F gaan in de periode, d.w.z. van $H_3C–CH_3$ naar $H_2N–NH_2$ naar HO–OH naar F–F, de activeringsbarrières afnemen en, interessanter, de activering van de F–F binding is zelfs barrièreloos. Naarmate we op de geselecteerde substraten van C naar F gaan, wordt het aantal substituenten rond de A–A binding kleiner, waardoor de katalysator het substraat gemakkelijk kan naderen, wat resulteert in afnemende activeringsbarrières. De oorzakelijke effecten van deze barrièrestabilisaties komen voort uit: (i) een verminderde activeringsspanning als gevolg van een zwakkere $H_nA–AH_n$ binding; (ii) een verminderde Pauli-afstoting als gevolg van een verschil in sterische afscherming van de $H_nA–AH_n$ binding; en (iii) een verbeterde backbonding-interactie tussen de bezette 4d atomaire orbitalen van de palladiumkatalysator en σ* acceptororbitaal van het substraat.

De bevindingen in dit proefschrift hebben het potentieel om experimentatoren uit te rusten met gedetailleerd mechanistisch inzicht dat een diepgaand begrip van de trends in reactiviteit van palladium-gemedieerde oxidatieve additiereacties kan vergemakkelijken.

Opsomming

Hierdie tesis fokus op die ondersoek van fundamentele oksidatiewe addisie (OA) reaksies wat deur palladium gekataliseer word (sien Hoofstuk 1). OA, synde die eerste en tempobepalende stap in kruiskoppelingsreaksies, is 'n reaksie van deurslaggewende belang in sintetiese chemie. Palladium-gekataliseerde kruiskoppelingsreaksies word alomgebruik in industriële toepassings, soos by voorbeeld in katalitiese omsetters en die sintese van geneesmiddels. Benewens hierdie toepassings, word palladium alomgebruik as 'n veelsydige katalitiese reagens in vele verskillende chemiese prosesse. Met inagneming van die belangrikheid van oksidatiewe addisiereaksies wat deur palladium gekataliseer word, is 'n diepgaande begrip van die onderliggende meganisme van kardinale belang om nuwe katalisators te ontwerp en die bestaandes te verbeter. In 'n neutedop is die hooffokus op die begrip van die meganisme agter die oksidatiewe-addisiestap en die neigings in aktiveringsenergiëe by variasie van óf die katalisator óf substraatstruktuur. Die volgende opsomming sal slegs die belangrikste bevindinge uit die betrokke hoofstukke bespreek.

Soos in Hoofstuk 2 verduidelik, is die bevindinge in hierdie tesis suksesvol verkry deur gebruik te maak van die 'Activation Strain Model' van chemiese reaktiwiteit (ASM, bespreek in Afdeling 2.3) in kombinasie met berekeninge gebaseer op Digtheidsfunksionaalteorie (DFT) soos geïmplementeer in die ADF program. Die ASM model is 'n fragment-gebaseerde benadering wat reaksies klassifiseer in terme van die rigiditeit en die bindingsvermoë van die oorspronklike reaktante, en die mate waartoe die reaktante langs die reaksieroete van 'n spesifieke reaksiemeganisme moet vervorm. Dus kan die totale energieprofiel van 'n bepaalde chemiese reaksie ontbind word na bydraes vanaf die vervorming van die reaktante (die vervormingsenergie) en hul onderlinge interaksies (die interaksie-energie). Die interaksie-energie kan dan verder ontleed word met behulp van die kanoniese energie-dekomposisie-analise (EDA) van ADF in elektrostatiese, destabiliserende Pauli-afstoting- en stabiliserende orbitaal-interaksies.

In Hoofstuk 3, met die doel om die onderliggende meganisme en neigings wat by die oksidatiewe byvoeging gevind word te verstaan, het ons ons kwantumchemiese verkenning van die palladium-gemedieerde aktivering van C(sp^n)–X bindings (n = 1–3; X = F, Cl, Br, I) in die argetipiese model-substrate $H_3C–CH_2–X$, $H_2C=CH–X$, en HC≡C–X deur middel van 'n model kaal-palladium katalisator uiteengesit. Eerstens het ons die bindingsdissosiasie-

entalpieë (BDE's) van die bindings wat geaktiveer moet word, ondersoek. Ons het dus by die C(sp^3)–X begin en daarna na C(sp^2)–X en uiteindelik na die C(sp)–X bindings beweeg vir elkeen van die geselekteerde stel X-atome hierbo. Ons het gevind dat soos wat ons in groep 17 afbeweeg, word die C(sp^n)–X-binding swakker en sodanig makliker om te breek. Gebaseer op ons gevorderde ontledingsmetodes, het ons ontdek dat wanneer die substituent X verander word, deur in Groep 17 af te gaan vanaf X = F na Cl na Br na I met betrekking tot die C(sp^n)–X substraat, die oksidatiewe-addisie-aktiveringsenergie drasties verminder word. Hierdie gunstige stabilisering van die aktiveringsenergie spruit uit twee faktore: (i) 'n minder destabiliserende aktiveringsspanning; en merkwaardiglik (ii) 'n gunstiger elektrostatiese aantrekking tussen die katalisator en die substraat. Indien die substraat van C(sp^n)–F na C(sp^n)–I verander word, word die elektrostatiese interaksie tussen die katalisator en substraat gevolglik ook gunstiger. Jodium, as die grootste halogeen uit die substituente, besit 'n meer diffuse- en elektronryk-digtheid wat op hulle beurt gunstiger elektrostatiese aantrekkings met onderskeidelik die palladiumkern en elektrondigtheid vorm. Hierdie effek maak dat die oksidatiewe addisiereaksies van die C(sp^n)–X bindings met groter halogeenatome met meer stabiliserende interaksies en dus laer reaksieaktiveringsenergie ooreenstem.

Vervolgens, in Hoofstuk 4 het ons die palladium-gemedieerde aktivering van $H_nA–AH_n$ bindings (AH_n = CH_3, NH_2, OH, F) deur katalisators PdL_n met L_n = geen ligand, PH_3 of $(PH_3)_2$ kwantum-chemies ondersoek. Hierin het ons gevind dat soos wat ons oor die reeks vanaf C tot F beweeg, d.w.s. van $H_3C–CH_3$ na $H_2N–NH_2$ na HO–OH na F–F, die aktiveringsenergie afneem en, meer interessant, die F–F binding kan totselfs sonder aktivering met die palladium reageer. Soos ons van C na F op die geselekteerde substrate beweeg, word die aantal substituente rondom die A–A binding minder en sodanig stel dit die katalisator in staat om die substraat met meer gemak te benader, wat lei tot dalende aktiveringsenergie. Die oorsaak van hierdie stabiliserings van die oorgangstoestande spruit uit: (i) 'n verminderde aktiveringsspanning as gevolg van 'n swakker $H_nA–AH_n$ binding; (ii) 'n verminderde Pauli-afstoting as gevolg van 'n verskil in steriese afskerming van die $H_nA–AH_n$ binding; en (iii) 'n verbeterde terugdonasie vanaf die besette 4d atoomorbitale van die palladiumkatalisator na die σ*-akseptororbitaal van die substraat.

Die bevindinge in hierdie tesis het die potensiaal om eksperimentele toe te rus met gedetailleerde meganistiese insig wat 'n diepgaande begrip van die neigings in reaktiwiteit van palladium-gemedieerde oksidatiewe addisiereaksies kan fasiliteer.

Acknowledgements

My PhD journey started on the 17th April 2018, with a few emails exchange: from **Myself**, directed to **Matthias** through **Henk** (Dr. Henk van den Heuvel, Director CIS-VU / Senior Advisor Higher Education management & organisation), then between **Matthias**, **Catharine**, and **Bryan**. All these happened in one good day and I was accepted in both **DATOC** (**SU**) and **TheoCheM** (**VU**) exciting groups!

I then applied for the **NRF-Nuffic**'s scholarship (National Research Foundation of South Africa-Nuffic's Netherlands Education Support Office (**NESO**), and without a doubt, my application was successful! From there, my real PhD journey **BEGAN**……...

First and foremost, immeasurable, and sincere gratitude are hugely indebted to my promoters, **Catharine** and **Matthias**, for granting me an opportunity to join your superb and wonderful research groups. Thank you for introducing me to the world of catalysis and affording me the opportunity to dwell much deep into the fascinating concept of cross-coupling reactions (specifically, oxidative addition reactions) research. Words cannot express my gratitude to acknowledge your unsurpassed knowledge, support, great patience you bestowed me during my PhD journey. You have always and still been making me feel at home under your research groups. I am truly fortunate to have you as a promoter and will forever be grateful and thankful for that. **Catharine**, I want to express my deepest appreciation for your unmatched support and motivational talks we used to have in your office. **Matthias**, I always enjoy your interactions and suggestions during our TheoCheM Friday's meeting – At times I'd be impatient for Fridays of the week to come, just to hear your theoretical broad and ever-sense making insights. This endeavour would not have been possible without your great and wonderful collaboration. And for ALL these, I say thank you. Keep your unmatched excellent work up!

To my co-promoter, **Trevor**!!! My sincere gratitude and heartfelt appreciation are immensely due to you. You accepted me from day one upon my arrival in the R-floor just after my intake meeting like a brother to this day. I would like to thank you for always seeking the best in me and for always asking those pressing and relevant basic research questions. To me, **Trevor**, you are such a *possibility catalyst*! Thank you for introducing me to the basics and a larger scale of chemical reactivity and theoretical chemistry. Thank you again for always

ensuring that some of my PhD work gets recognized and published to the entire science community. Your forever professional assistance will never go unnoticed and for that, I say thank you….!

Célia, although you were not directly involved in my PhD journey, however, your indirect crucial contributions during the virtual Fridays' TheoCheM meetings will never go unnoticed. And for all these, I say thank!

Dalla Tiezza, heartfelt gratitude goes to you my friend, **Marco,** for always creating out time to reply to my e-mails, for being so kind to show interest in my research and for giving me so ever-sense making suggestions, particularly in my results from the inception of manuscripts preparations, and for that, I say thank you!

I am highly indebted and thoroughly grateful to you, **Pascal**, for always acknowledging and finding time to reply to my emails and "Slacks". Your fresh experience in the PhD and research journeys should not go unnoticed, you really paved an EVEN PATH to my first and second manuscripts in the group. To me, professionally, **P**..…You are the "*perfection personified*". And for all these, I say thank you brother!

Song, I would like to acknowledge my humble gratitude to you for always been there to listen and help me out in some of my stumbling blocks of research. And most importantly, to always agreeing to our special zoom conversations of my research. And for all these, **Dr. Yu**, I say thank you…….!

Celine, **Dani**, **Eva**, **Eveline, and Lucas** why would I forget you guys? You welcomed me in our lab space with your whole warm-hearts and never for a single day have I felt left out or neglected! Your direct and indirect contributions will forever ring a bell in my mind. For all these, I say thank you!

My sincere and humble gratitude goes out to **all** the **TheoCheM** group colleagues. I enjoyed every biddest of always being around all of you, and of-course our crucial Fridays' virtual meetings. For that, I say thank you, **Ayush**, **Celine**, **Dani**, **Eva**, **Eveline**, **Ken**, **Lucas**, **Nicolai**, **Pau**, **Stephanie**, **Steven**, **Thomas**, **Xiaobo**, for your direct and indirect contributions to my research.!

Brigitte, my sincere gratitude goes out to you for your usual and prompt replies to my emails. I'm thankful of you for always making sure that am settled fully in my lab provided space. Please continue helping us when we are at our home Universities. For this, I say thank you, **Brigitte**!

I would like to extend my sincere gratitude to the members of **DATOC** and **Supramolecular Materials Research Groups**. Thank you, **Alan**, **Dewald**, **Oluwatoyin**, **Shane**, and **Somananda**.

Thank you to my friend and academic sister, **Charlotte Mamogobo**, for our usual talks and walks over lunch on the journeys of our PhDs.

To my family: Godimo ga tše ka moka, ke rata go leboga, **badimo** ba gešho, **boMma (Mapitsi Maiša 'a Raletladi)**, **boPapa (Moloko wa lebadi)** ba baithobaletšeng boroko byo botelele, **bo buti**, le **bo sesi**, le **batlogolo baka**, ka go mpha maatla le hlohloletšo mo go dithutong tšaka. Kere Modimo a nhlokomeleleng lena le go leshigofatša, gomme, a lefe BOHLALE. And to my girlfriend, **Lerato**, ke leboga hlohloletšo ya gago ye o mphileng yona sa le ke thoma go tsena sekolo ka 2019. Modimo a go dire sentle!!

And finally, I would like to thank the **University of Limpopo** for granting me a four-year study leave to pursue my PhD degree as part of young staff development. My special thanks go out to my former Head of Department (HoD), **Dr. Mary Thomas**, for approving my leave application – And not forgetting my current HoD, **Prof. Richard Mampa**, for his full support during my final Ph.D. finishing touches. The Executive Dean of the Faculty of Science and Agriculture, **Prof. Hlengani Siweya,** to also approving my request plus some lengthy conversations we had before my departure, and lastly, the Vice-Chancellor and principal (Hlogo), **Prof. Mahlo Mokgalong**, for his final approval and closure of my leave request.

List of Publications

Part of this work

Palladium-Catalyzed Activation of Carbon–Halogen Bonds: Electrostatics-Controlled Reactivity

B.P. Moloto, P. Vermeeren, M. Dalla Tiezza, C. Esterhuysen, F.M. Bickelhaupt, T.A. Hamlin

Eur. J. Org. Chem. **2022**, 184–190

DOI: 10.1002/ejoc.202200722

Palladium-Catalyzed Activation of $H_nA–AH_n$ Bonds (AH_n = CH_3, NH_2, OH, F)

B.P. Moloto, P. Vermeeren, M. Dalla Tiezza, T. Bouwens, C. Esterhuysen, T.A. Hamlin, F.M. Bickelhaupt

Pure and Applied Chemistry, **2023**, *95*, 181–191

DOI: https://doi.org/10.1515/pac-2022-1004

Not Part of this work

Palladium-Catalyzed Activation of Polar Bonds: From Strain Control to Interaction Control

W.-J. van Zeist, L.P. Wolters, B.P. Moloto, P. Vermeeren, C. Esterhuysen, T.A. Hamlin, F.M. Bickelhaupt

Manuscript to be submitted.

Conferences

Not part of this work

ISXB4 – *4th International Symposium on Halogen Bonding*

Stellenbosch, South Africa, 2 – 6 November 2020

Poster and flash oral presentation: *Nature of the Covalent Bonding in Gold-Chalcogen Complexes.*

Part of this work

VCCA – *Virtual Conference on Chemistry and its Applications*

University of Mauritius, Mauritius, 8 – 12 August 2022

Best oral presentation: *Palladium-Catalyzed Activation of Carbon–Halogen Bonds: Electrostatics-Controlled Reactivity.*

YCS (WC) – *Young Chemist Symposium (Western Cape)*

Stellenbosch University, South Africa, 9 September 2022

Best poster presentation: *Palladium-Catalyzed Activation of Carbon–Halogen Bonds: Electrostatics-Controlled Reactivity.*